UNIVERSITÉ DE SHERBROOKE

Faculté des lettres et sciences humaines

Département de géomatique appliquée

Identification and characterization of natural aerosols over the Arctic

Keyvan Ranjbar

Thesis submitted in partial fulfilment of the requirements for the degree of Doctor of Philosophy (Ph.D.) in Remote Sensing

JURY

Supervisor: Prof. Norman T. O'Neill

Internal Member: Prof. Alain Royer

Internal Member: Prof. Yannick Huot

External Member: Prof. Carlos Toledano

Abstract

Global warming is one of the most serious challenges that we face today. The Arctic is particularly vulnerable to its effects. Aerosols play a key role in terms of their radiative forcing effects (both directly and indirectly in terms of their influence on clouds). They are, accordingly, one of the greatest uncertainty sources in climate modelling inasmuch as their microphysical, chemical and optical characteristics are not well understood.

Arctic aerosols can be categorized into anthropogenic and natural aerosols. Natural aerosols include black and brown carbon (BC and BrC), dust, sea-salt, volcanic sulphates and ash as well as level Ib polar stratospheric clouds (PSCs). The ultimate goal of the research project was to characterize the optical and microphysical properties of natural aerosols within the constraints of being able to capture specific events of opportunity. While we investigated numerous natural aerosol events over the Arctic, we eventually focussed on two extraordinary events.

In Paper 1, we employed ground-based sunphotometry, ground-based FTIR (Fourier Transform IR) retrievals, lidar profiles, satellite remote sensing and aerosol modelling to analyze an extreme, August-2017 smoke event over Eureka that was driven by pyrocb (extreme convection) fires near Prince George, BC. This paper was, we believe, an innovative and original contribution on various levels: first and foremost, in terms of the event as well as the instrumental infrastructure and expertise that we developed and brought to bear over many years at Eureka. It was also original in terms of the production of a 10-year τ_f (fine mode optical depth) smoke climatology that excluded confounding events such as the 2008 and 2009 Kasatochi and Sarychev stratospheric intrusions of fine mode sulphates. An original constraint on the labelling of τ_f events as smoke events was the correlation between τ_f and FTIR-retrieved CO abundance (CO being a classical smoke product). To demonstrate the extreme nature of the event we employed a "peak over threshold" (POT) analysis of individual τ_f peaks during our 10-year sampling period.

Paper 2 was arguably the most significant and original contribution. It involved the successful application of remote sensing techniques to detect a low-altitude, high-Arctic (81 °N) dust plume over Lake Hazen (Ellesmere Island) using a diverse array of passive and active, satellite-based remote sensing techniques. We are not aware of any published remote sensing investigations of

local Arctic dust carried out over the complex surface of snow, ice and dust that was encountered in the Lake Hazen case. We exploited multi-angle and multi-spectral imaging capabilities (MISR and MODIS imagery) as well as the particle size dependant profiling capabilities of active sensors (the CALIOP lidar and the CloudSat radar) to identify and characterize the key physical and optical properties of the dust plume. This was accomplished in spite of the fact that the remote sensing algorithms of all these sensors were not adapted to Arctic conditions. We succeeded in characterizing the upper plume thickness (the region of highest signal-to-noise) in terms of 532 nm optical depth (~ 0.7) and the effective radius of the plume particles (between 18 and 25 μm in radius; what the dust community characterize as "giant" dust particles).

Résumé

Le réchauffement climatique est l'un des défis les plus graves auxquels nous sommes confrontés aujourd'hui. L'Arctique est particulièrement vulnérable à ses effets. Les aérosols jouent un rôle clé en termes d'effets de forçage radiatif (à la fois directement et indirectement en termes d'influence sur les nuages). Par conséquent, ils sont l'une des plus grandes sources d'incertitude dans la modélisation du climat dans la mesure où leurs caractéristiques microphysiques, chimiques et optiques ne sont pas bien comprises.

Les aérosols arctiques peuvent être classés selon deux catégories: les aérosols anthropiques et les aérosols naturels. Les aérosols naturels comprennent le carbone noir et le carbone brun (BC et BrC), la poussière, le sel de mer, les sulfates volcaniques et les cendres ainsi que les nuages stratosphériques polaires de niveau Ib (PSC). Le but ultime du projet de recherche était de caractériser les propriétés optiques et microphysiques des aérosols naturels dans les contraintes de pouvoir capturer des événements d'opportunité spécifiques. Bien que nous ayons enquêté sur de nombreux événements d'aérosols naturels dans l'Arctique, nous nous sommes finalement concentrés sur deux événements extraordinaires.

Dans le premier article, nous avons utilisé la photométrie solaire au sol, les récupérations au sol FTIR (Fourier Transform IR), les profils lidar, la télédétection par satellite et la modélisation des aérosols pour analyser un événement de fumée extrême en août 2017 sur Eureka, entraîné par le incendies pyrocb (convection extrême) près de Prince George, en Colombie-Britannique. Selon nous, cet article a été une contribution innovante et originale à divers égards: d'abord en termes d'événements d'aérosols ainsi que l'infrastructure instrumentale et l'expertise que nous avons développées et apportées au fil des années sur Eureka. L'article était également original en termes de production d'une climatologie des fumées τ_f (profondeur optique en mode fin) sur 10 ans qui excluait les événements confondants tels que les intrusions stratosphériques de sulfates en mode fin de Kasatochi et Sarychev de 2008 et 2009. Une contrainte originale sur l'étiquetage des événements τ_f en tant qu'événements de fumée était la corrélation entre τ_f et l'abondance de CO récupérée par FTIR (le CO étant un produit de fumée classique). Pour démontrer la nature extrême de l'événement, nous avons utilisé une analyse ''pic au-dessus du seuil'' (Peak Over Threshold, POT) des pics τ_f individuels au cours de notre période d'échantillonnage de 10 ans.

Le deuxième article était sans doute la contribution la plus importante et la plus originale de ce projet. Elle impliquait la réussite de l'application de techniques de télédétection pour détecter un panache de poussière à basse altitude et dans l'Extrême-Arctique (81 °N) au-dessus du lac Hazen (Ellesmere Island) en utilisant plusieurs techniques de télédétection passives et actives par satellite. Nous n'avons connaissance d'aucune publication traitant de la télédétection de la poussière locale de l'Arctique effectuée sur la surface complexe de neige, de glace et de poussière telle que présente au lac Hazen. Nous avons exploité les capacités d'imagerie multiangles et multispectrales (imagerie MISR et MODIS) ainsi que les capacités de profilage dépendantes de la taille des particules des capteurs actifs (le CALIOP lidar et le radar CloudSat) pour identifier et caractériser les propriétés physiques et optiques clés du panache de poussière. Cela a été accompli malgré le fait que les algorithmes de télédétection de tous ces capteurs n'étaient pas adaptés aux conditions arctiques. Nous avons réussi à caractériser l'épaisseur du panache supérieur (la région du signal comportant le bruit le plus élevé) en termes d'épaisseur optique à 532 nm (~ 0.7) et le rayon effectif des particules du panache (entre 18 et 25 µm de rayon; ce que les spécialistes du domaine qualifient de particules de poussière ‘‘géantes’’).

Acknowledgments

Foremost, I would like to express my sincere gratitude to my supervisor, Professor Norman T. O'Neill for his vast contribution to my thesis, for his motivation, enthusiasm and patience, for granting me his confidence and most importantly, his friendship throughout my PhD. You guided me to have a more scientific thoughts, which I am truly grateful and indebted. I would like to thank you for keeping an open door for me all the time, urging me to perfect my research, as well as filling our collaboration at all levels with pleasure. I could not have had a better supervisor.

I am grateful to Professor Alain Royer, Professor Yannick Huot, and Professor Carlos Toledano who kindly agreed to be jury members for my thesis during this tough time (Corona virus pandemic).

I would like to thank my lab mates for the scientific discussions and for all the fun we have had in the last four years.

I would like to say a big thank you to my family and especially to my parents for their unconditional love and support. Last but not least, no words can express my gratitude towards my wife, Arezoo, for her love, support and patience during my study.

To my beloved wife, Arezoo

To my parents

Table of Contents

Sommaire en français

Le réchauffement climatique est l'un des défis les plus importants auxquels le monde est confronté aujourd'hui. L'Arctique est particulièrement vulnérable aux effets de ce réchauffement et divers indicateurs de durabilité ont rapidement décliné au cours des dernières décennies. Depuis plusieurs années, l'augmentation de la température dans l'Arctique est deux fois plus élevée que pour des latitudes plus basses (IPCC, 2013). La fonte de la glace de mer et la libération de méthane sont ainsi deux des manifestations les plus évidentes de ce changement (Serreze et al., 2007) et peuvent affecter tous les climats dans leur ensemble. Par conséquent, la surveillance et l'étude des facteurs environnementaux dans l'Arctique sont susceptibles de fournir des indicateurs pour une détection précoce des futurs changements climatiques (Stocker, 2013).
Parmi ces facteurs, les aérosols ont ainsi un impact important sur cette région du globe. En effet, les courants d'air mondiaux dominants font de l'Arctique une zone de dépôt privilégiée pour les polluants atmosphériques en provenance des basses latitudes (Stohl, 2006). La concentration des polluants à certains endroits dépasse ainsi les niveaux trouvés dans les zones urbaines densément peuplées (Stocker, 2013).

La définition des aérosols, de leurs propriétés et de leurs interactions atmosphériques telles qu'énoncées dans Hind (1999) sont communément employées dans la littérature. L'auteur définit un aérosol comme "*une suspension de particules solides ou liquides dans un gaz*" (Hind, 1999). Il note en outre que le rayon de ces particules varie d'une fraction de micron à quelques dizaines de microns. Selon les facteurs d'émission et de transport, leur durée de vie atmosphérique peut varier de quelques secondes à environ un an.

Les aérosols interagissent avec la lumière du soleil via les mécanismes optiques de diffusion et d'absorption. Ils redirigent atténuent l'énergie lumineuse en fonction de la longueur d'onde et du faisceau lumineux donné. Ce concept général mène aux formulations des paramètres microphysiques (taille et forme), des paramètres chimiques et optiques (diffusion, absorption et atténuation / extinction) qui caractérisent tout aérosol ou tout groupement d'aérosols dans l'atmosphère.

Les particules d'aérosol peuvent être caractérisées par leurs propriétés extensives et intensives. Les propriétés extensives se réfèrent à la quantité d'aérosol (comme la densité de nombre de PSD

(Particle Size Distribution)) tandis que les propriétés intensives se rapportent aux paramètres par particule (ou aux moyennes des paramètres par particule à travers le PSD). Bien que les effets optiques dominants des aérosols soient associés à des propriétés extensives des aérosols, leurs propriétés intensives peuvent également être importantes.

Le paramètre optique le plus important concernant les effets radiatifs atmosphériques, que ce soit étudié depuis le sol ou par imagerie satellitaire (extensive), est l'épaisseur optique des aérosols (AOD). Il décrit en grande partie l'effet de diffusion des aérosols dans la partie réfléchissante du spectre solaire car la composante d'absorption de l'AOD dans ce régime est généralement faible. L'AOD et les paramètres dérivés de la forme spectrale de l'AOD peuvent par ailleurs être divisés en ses composantes extensives et intensives en mode fin et grossier. Les paramètres extensifs incluent (cf. O'Neill et al., 2003) l'AOD en mode total, fin et grossier, tandis que les paramètres intensifs incluent (générique) l'exposant Angstrom total (une régression linéaire classique du premier ordre sur plusieurs longueurs d'onde), la pente spectrale en mode fin et grossier à une longueur d'onde donnée, un rayon efficace en mode fin et grossier, et une fraction en mode fin (FMF; le rapport entre l'AOD en mode fin et l'AOD totale).

L'énergie fournie par le soleil régit en grande partie les climats de la Terre, mais ne parvient pas en intégralité à sa surface. Les aérosols induisent des effets de rétrodiffusion et d'absorption importants qui ont un impact direct sur le forçage radiatif du système surface-atmosphère (ce qu'on appelle communément *l'effet direct*; voir par exemple IPCC, 2013). Ces effets dépendent du type d'aérosol, les sulfates et nitrates reflètent ainsi une fraction importante du rayonnement et consécutivement refroidissement l'atmosphère. En revanche, le carbone noir est un absorbeur puissant et entraîne un réchauffement de l'atmosphère. Le deuxième effet majeur de forçage radiatif des aérosols (*l'effet indirect*) est dû à leur rôle de nucléation dans la formation de particules des nuages (gouttelettes d'eau ou cristaux de glace). Les variations des propriétés extensives et intensives des aérosols peuvent donc avoir des conséquences importantes sur les propriétés microphysiques des nuages, leurs propriétés de forçage radiatif, leur durée de vie, etc. (ibid). Les aérosols sont l'une des plus grandes sources d'incertitude dans la modélisation climatique puisque leurs caractéristiques microphysiques, chimiques et optiques, et donc leurs effets directs et indirects, ne sont pas bien caractérisés (ibid).

Les aérosols de l'Arctique peuvent être classés en aérosols anthropiques et naturels (Shaw, 1995). Au-dessus de l'Arctique, les aérosols anthropiques sont largement associés au phénomène de brume arctique. Cet effet culmine à la fin de l'hiver / au début du printemps. Il est le résultat du "bol Arctique", dans lequel les sources de pollution sont étendues plus au sud pendant l'hiver polaire (voir Law & Stohl, 2007 par exemple). Ces types d'aérosols ont des concentrations plus élevées en sulfates, en matière organique (OM) et en carbone noir (BC) par rapport aux aérosols naturels (Quinn et al., 2008).

Les aérosols naturels, qui forment le principal objet de cette thèse, comprennent:

- Les aérosols de carbone noir (BC) et de carbone brun (BrC). La source la plus évidente de ces aérosols dans l'Arctique est la fumée de la combustion de biomasses dans les régions du sud (e.g. O'Neill et al. (2008) et Myhre et al. (2007))
- Les poussière (typiquement supramicronique), généralement dues à l'érosion éolienne sur les déserts chinois et / ou à la poussière africaine (Zwaaftink et al., 2016) mais aussi à l'érosion locale estivale dans l'Arctique (Bullard et al., 2016)
- Le sel marin généré par des vents violents sur les eaux océaniques (Jaeglé et al., 2011).
- Les sulfates volcaniques submicroniques (O'Neill et al., 2012) provenant de la condensation de gaz SO2 émis par des volcans en éruption.
- Les nuages stratosphériques polaires de niveau Ib (PSC) (Pitts et al., 2011). Ces aérosols sont généralement formés de sulfates volcaniques submicroniques qui ont pénétré dans la stratosphère.

La télédétection au sol, appuyée par la télédétection satellitaire, est un moyen essentiel de surveillance des aérosols. La télédétection passive et active au sol peut fournir une complémentarité aussi bien qu'une redondance des informations qui permettent l'extraction de presque tous les paramètres essentiels et robustes des aérosols qui influencent le budget de transfert radiatif local.

Il y a relativement peu d'analyses de télédétection satellitaire dans la région de l'Arctique parce que les recherches d'AOD dans cette région sont en général problématiques (voir article 2). O'Neill et al. (2012) ont utilisé des mesures au sol telles que la sunphotométrie, l'Arctic High Spectral Resolution Lidar (AHSRL) et le CANDAC Rayleigh-Mie-Raman Lidar (CRL), et des images

satellitaires telles que CALIOP, MODIS et OMI pour étudier les effets de l'éruption volcanique de Sarychev en 2009 sur l'Arctique. Tomasi et al. (2015) ont utilisé MODIS, MISR et AATSR pour retrouver l'épaisseur optique des aérosols (AOT) sur de grandes parties des régions polaires océaniques durant le printemps et l'été. Di Pierro et al., (2013) ont utilisé CALIOP pour examiner la variabilité verticale, horizontale et temporelle des aérosols troposphériques dans les régions arctiques au cours de la période entre 2006-2012.

Concernant la question spécifique des aérosols naturels, presque tous les articles mentionnés sur la télédétection au sol se concentrent sur l'influence printanière des poussières asiatiques (soit sous la forme d'une diminution significative de l'exposant d'Angstrom, soit d'une augmentation significative de l'AOD en mode grossier). AboEl_Fetouh et al. (2020) ont montré que ces effets optiques pourraient être associés à un petit pic de mode grossier (du PSD) d'un rayon d'environ 1,3 µm. Stone et al. (2014) ont fait état de l'influence probable de l'AOD en mode grossier des aérosols de sel marin à Barrow, en Alaska. Dans le premier article, nous avons utilisé la sunphotométrie au sol, les récupérations au sol FTIR (Fourier Transform IR), les profils lidar, la télédétection satellitaire et la modélisation des aérosols (NAAPS) pour analyser un événement de fumée extrême sur Eureka, provoqué par des incendies de pyrocb (convection extrême) près de Prince George, Colombie-Britannique. Dans le deuxième article, nous avons présenté la détection sans précédent d'un panache de poussière local (basé uniquement sur des recherches par satellite) induit par le flux de drainage le long des bassins fluviaux glaciaires. Ce flux est produit par la dynamique de l'air froid des glaciers de haute altitude entourant le lac Hazen (situé dans le nord d'Ellesmere Île de l'Extrême-Arctique).

L'identification et l'étude des aérosols naturels au-dessus d'Eureka (et d'autres sites d'opportunité) tels que les aérosols de fumée, les aérosols volcaniques, la poussière, le sel de mer et les PSCs de niveau Ib formaient l'objectif initial de cette recherche. Le but ultime était de caractériser les propriétés optiques et microphysiques des échantillonnages représentatifs d'aérosols naturels à partir des événements spécifiques au cours des dernières années.

L'hypothèse générale d'origine était que les données de télédétection au sol, appuyées par des informations auxiliaires telles que les données de télédétection par satellite, les données sur les aérosols de surface et les simulations de modèles, pouvaient être utilisées pour caractériser

adéquatement et comprendre correctement les propriétés des différents aérosols naturels dans l'Arctique. Par "caractériser adéquatement", nous entendons que l'analyse par télédétection démontrerait un niveau acceptable de précision et de robustesse (sans limitation par les incertitudes des données) et qu'elle présenterait une redondance et une corrélation physiquement défendables avec d'autres sources indépendantes d'information.

Alors que nous avons considéré de nombreux événements d'aérosols naturels au-dessus de l'Arctique, nous nous sommes finalement concentré sur deux événements extraordinaires qui étaient d'un intérêt plus général.

L'article 1 est un article original, et selon nous innovant, publié dans *Atmospheric Environment*. Il traite d'un événement de fumée extrême observé sur Eureka en août 2017. Son originalité provient de l'importance de l'événement étudié (la plus grande épaisseur optique jamais mesurée sur Eureka) et de l'infrastructure instrumentale et de l'expertise que nous avons développée depuis de nombreuses années sur la zone d'étude Eureka. L'article était également original en termes de la production d'une climatologie de τ_f (épaisseur optique en mode fin) associée à la fumée sur 10 ans (basée sur les données AEROCAN / AERONET collectées sur nos deux sites à Eureka) qui excluait des événements tels que les Kasatochi de 2008 et 2009 et l'intrusion stratosphérique de sulfates en mode fin de Sarychev. Une contrainte supplémentaire et originale sur l'étiquetage des événements τ_f en tant qu'événements de fumée était la corrélation entre τ_f et l'abondance de CO mesurée (une forte corrélation étant une indication de fumée étant donné que le CO est un produit classique des feux de biomasse). Le niveau de corrélation observée est, à notre connaissance, sans précédent. Particulièrement en présence de fortes variations de la profondeur optique des nuages, il témoigne ainsi de la fiabilité de la méthode de récupération (la récupération SDA d'AERONET). Pour démontrer la nature extrême de l'événement, nous avons utilisé une analyse ‘‘pic au-dessus du seuil’’ (POT) des pics τ_f individuels au cours de notre période d'échantillonnage de 10 ans. Ce processus impliquait une analyse minutieuse de tous les événements de fumée importants au cours de cette période et la conversion de cette analyse manuelle en une routine automatique d'extraction de tous les événements de fumée au-dessus d'un certain seuil τ_f. Cette routine a ainsi généré une distribution des événements de fumée extrêmes à partir laquelle l'inférence statistique d'un extrême significatif a pu être tirée. Même si l'événement d'août 2017 ne s'est pas avéré être un événement

extrême en termes de moyenne mensuelle simple, cette observation confirme l'idée que des statistiques sur les événements extrêmes sont nécessaires pour démontrer leur caractère unique. Nous avons également utilisé des profils historiques (2005-2010) AHSRL pour estimer une hauteur de panache de fumée optiquement moyenne de ~ 3 à 3 ½ km au printemps et en été.

L'article 2 est sans doute la contribution la plus importante et la plus originale. Elle implique l'application, avec succès, de techniques de télédétection passive et active par satellite pour détecter un panache de poussière à basse altitude au-dessus du lac Hazen dans l'Extrême-Arctique. Nous n'avons pas connaissance d'études de télédétection publiées sur la poussière locale de l'Arctique: la télédétection d'un panache de poussière au-dessus d'une surface complexe de neige, de glace et de poussière déposée sur cette surface est au mieux difficile. Nous avons exploité les capacités d'imagerie multi-angles (MISR) et multispectrales (visible aux infrarouges thermiques) (MODIS) ainsi que les capacités de profilage de capteurs actifs (le lidar CALIOP et le radar CloudSat) pour identifier, localiser et caractériser les principales propriétés physiques et optiques du panache de poussière. Ce processus a été accompli malgré le fait que les produits de télédétection de ces capteurs n'étaient pas adaptés aux conditions de l'Arctique (aucun de ces produits n'indiquait la nature des poussières du panache). Finalement, nous avons réussi à caractériser l'épaisseur du panache supérieur (la région du signal au bruit le plus élevé) en termes d'épaisseur optique de 532 nm (~ 0,7) et le rayon effectif des particules du panache (entre 18 et 25 µm de rayon; ce que les spécialistes du domaine qualifie de particules de poussière ''géantes''). Ces événements de poussières locales, considérés comme des phénomènes réguliers de fin d'été et de début d'automne au-dessus de l'Arctique, ont été reconnus comme d'importants contributeurs à la dynamique des aérosols à l'échelle de l'Arctique et aux effets de forçage radiatifs associés. Pour ce dernier cas, nous avons produit des images dérivées de MODIS sur le lac Hazen et l'île d'Ellesmere qui ont mis en évidence les effets d'assombrissement (réduction de l'albédo) probablement dus à ces évènements. L'impact de l'absorption sur la fonte de neige et de glace aux hautes latitudes a été reconnu comme un effet de rétroaction positive potentiellement important (Bullard et al.2016).

1. Introduction

Global warming is one of the most serious challenges that the world is facing today. The Arctic is particularly vulnerable to its effects and various sustainability indicators have been found to be declining rapidly in the last few decades. In recent years, the average Arctic temperature increase was reported to be double that found at more southerly latitudes (IPCC, 2013). Figure 1 shows both the "Arctic amplification" of average temperature increase as well as an increase in the uncertainty of that increase with increasing latitude (ibid). In fact, because different processes in the Arctic climate system are not sufficiently understood, they are poorly represented in climate models. Our understanding of Arctic climate processes is limited by a scarcity of observations in the Arctic region, especially during the polar winter (when 24-hour darkness or dusk conditions are predominant for a period that is a function of time and Arctic latitude).

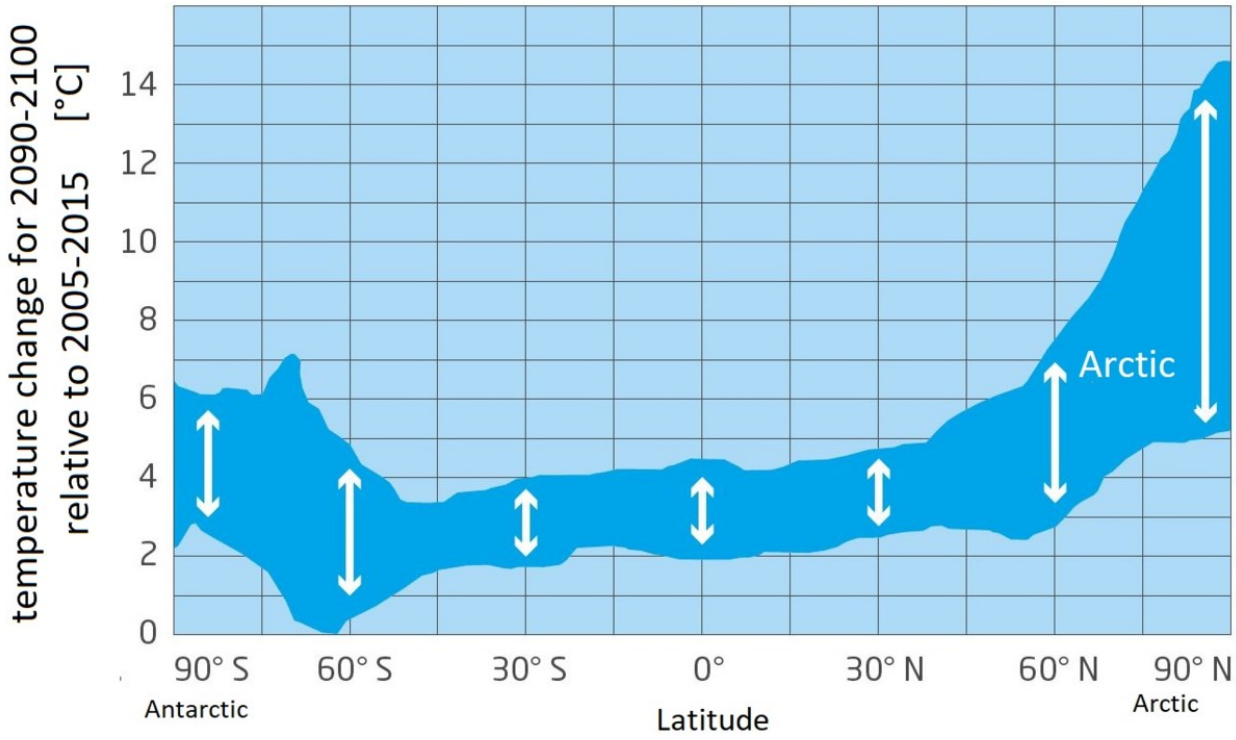

Figure 1 Projected warming by the end of the century as a function of the latitude. The envelope of uncertainty represents the range or projections for a variety of different models (Graphic: The mission of MOSAiC, https://mosaic-expedition.org/science/mission/).

Maybe the most spectacular results are the sea ice loss and Arctic methane release (Serreze *et al.*, 2007). These changes can significantly affect the whole planet through their impacts on global climate. Therefore, the monitoring and study of environmental factors in the Arctic are likely to provide indicators for early detection of future climate changes (IPCC, 2013).

Aerosols (defined immediately below) are the overwhelming source of Arctic pollution. The dominant global air currents make the Arctic area the fallout region for long-range transport of air pollutants from low latitudes (Stohl, 2006). As a consequence, the pollutant concentration in some Arctic regions exceeds the levels found in densely polluted urban areas (IPCC, 2013). Anthropogenic emissions from northern Eurasia (the predominant source of the Arctic haze discussed below) have been identified by model simulations, surface, airborne and remote sensing measurements as the principal source for the seasonal aerosol variations observed in the Arctic background (Warneke *et al.*, 2010). Shindell et Faluvegi, (2009) found that 1.1°C of the 1.5°C Arctic increase that occurred over the past three decades relates to the regional aerosol composition. They also found that improvements in air quality in Europe and the United States caused a decrease in sulfate and black carbon (BC) aerosol, while anthropogenic emissions in Asia increased BC in the Arctic.

A common source for the definition of aerosols, their properties and their atmospheric interaction, (and the general source for the affirmations made in this paragraph) is Hinds (1999). The author defines an aerosol as "A suspension of solid or liquid particles in a gas". He further notes that these particles vary in radial size from a small fraction of a micron to tens of microns. Depending on emission and transport factors, their atmospheric lifetime may vary from a ~few seconds to ~ year.

Aerosols interact with sunlight via the optical mechanisms of scattering and absorbing. They redirect light energy (scattering) and attenuate light (absorption and out-scattering for a given beam of light). This general concept leads to formulations of microphysical parameters (size and shape[1]), chemical parameters and optical parameters (scattering, absorption and attenuation/extinction) that characterize any aerosol or any grouping of aerosols in the atmosphere. Basic texts on aerosol optical parameters are numerous in the literature. One classic text on spherical, single-particle

[1] Particle shape is a 2nd microphysical parameter, but in lieu of particle shape information, spherical particles are the default shape assumed for aerosols

aerosol optical parameters of scattering, absorption and attenuation (cross sections) is Deirmendjian (1969). This author defines the two critical microphysical and optical parameters (respectively particle size and complex refractive index[2]) determining spherical aerosol optical parameters. A good text that combines per-particle aerosol optical parameters, volumetric aerosol optical parameters (per unit volume optical parameters labelled as coefficients), columnar optical parameters and general atmospheric radiative transfer concepts is Hansen & Travis (1974). The transformation from per-particle optical parameters to volumetric optical parameters is achieved by integrating the former over the particle size distribution (PSD) of aerosols at some point in the atmosphere (where the PSD is effectively a histogram of particle size). These volumetric parameters are then integrated over altitude to yield columnar parameters (the basic entity employed in passive ground- and satellite-based remote sensing)

A working hypotheses that motivates much of our investigations is that the impact of aerosols in the solar reflective part of the spectrum (roughly 0.4 to 4 μm) is essentially bimodal: one can divide aerosols into fine (sub-micron or accumulation) and coarse (super-micron) PSDs that largely describe their optical influence (see, for example, O'Neill et al., 2001 and references cited therein). This bi-modality feature is generally a consequence of the primary or secondary formation mechanisms of different species of aerosols (respectively, aerosols formed by atmospheric chemical reactions versus aerosols that are introduced directly into the atmosphere; see Hinds, (1999), for example). The division into fine and coarse mode aerosols is thus strongly linked with formation mechanism (for example, secondary aerosols are generally fine mode while primary aerosols can be both coarse or fine mode in nature).

Aerosol particles can be characterized by their extensive and intensive properties. Extensive properties refer to aerosol amount (the fundamental microphysical example being PSD number density[3]) while intensive properties relate to per-particle parameters (or averages of per-particle parameters across the PSD). While the dominant optical effects of aerosols are associated with extensive properties of aerosols, their intensive properties can also be important.

[2] A function of particle chemistry
[3] or alternate PSD number density formulations such as PSD volume density

The single most important aerosol optical parameter from a standpoint of general atmospheric radiative effects and from a standpoint of ground- and satellite-based remote sensing is (extensive) aerosol extinction optical depth or (AOD). It largely describes the out-scattering effect of aerosols in the solar reflective part of the spectrum since the absorption component of the AOD in that regime is typically small. The AOD and parameters derived from the spectral shape of the AOD can be divided into fine and course mode, extensive and intensive components. Extensive parameters include (c.f. O'Neill et al., 2003) total, fine and coarse mode AOD while intensive parameters include total (generic) Angstrom exponent (a classical, first order linear regression over multiple wavelengths), fine and coarse mode (true spectral) derivatives at a specific wavelength, fine and coarse mode effective radius, and fine mode fraction (FMF; the ratio of fine mode AOD to total AOD).

The sun provides the energy that drives earth's climate: but not all of this energy finds its way to the surface. The mechanisms and effects of climate change are the most studied phenomena of our time. Aerosols induce significant backscatter and absorption effects that directly impact the radiative forcing effects on the surface–atmosphere system (what is commonly known as the direct effect; see for example, IPCC,2013). These effects are species dependant: for instance, sulfates and nitrates reflect a significant fraction of radiation and generally result in cooling of the atmosphere. In contrast, black carbon is a strong absorber and generally result in atmosphere warming. The second major climate forcing effect of aerosols (the indirect effect) is due to their role as nucleation and ice forming nuclei in the formation of cloud particles (water droplets or ice crystals): variations in the extensive and intensive properties of aerosols can have important influences on the microphysical properties of clouds, their radiative forcing properties, their lifetime, etc. (ibid). Aerosols are one of the greatest uncertainty sources in climate modelling (i.e. a significant contribution to the uncertainty seen in Figure 1) inasmuch as their microphysical, chemical and optical characteristics and thus their direct and indirect effects are not well characterized (ibid).

Arctic aerosols can be categorized into anthropogenic and natural aerosols (Shaw, 1995). Anthropogenic aerosols over the Arctic are largely associated with the phenomenon of Arctic haze, an effect which peaks in the late winter / early spring and which is the result of the ‘‘Arctic bowl’’ wherein contributions from pollutions sources are extended further south during the Polar winter

(see Law & Stohl, 2007 for example). These types of aerosols have higher concentrations of sulphates, organic matter (OM) and black carbon (BC) with respect to natural aerosols (Quinn *et al.*, 2008).

Natural Arctic aerosols, the general overall motivation for this thesis, include:

- Black carbon (BC) and brown carbon (BrC) aerosols. The most apparent source of such aerosols in the Arctic is smoke from biomass burning in the southern regions (see for example Tomasi et al., 2007 and Myhre et al., 2007)
- Dust (typically super micron), generated by wind erosion in Chinese and mid-eastern deserts and/or the Saharan desert (Zwaaftink et al., 2016) but also from local, summertime erosion in the Arctic (Bullard et al., 2016)
- Sea-salt generated by high winds over oceanic waters (Jaeglé et al., 2011).
- Volcanic, sub-micron sulphates (see, for example, Hoffman et al., 2010) from the condensation of volcanic-emitted SO_2 gas and resulting from explosive eruption mechanisms.
- Level Ib polar stratospheric clouds (PSCs) (see, for example, Pitts et al., 2011). These aerosols are generally formed from sub-micron volcanic sulphates that have made their way into the stratosphere.

Ground-based remote sensing, supported by satellite-based remote sensing is a critical means of monitoring aerosols: it provides a "macro-averaged" characterization of aerosol properties that makes up for, in terms of its more robust (columnar) perspective, what it lacks in detail (as compared to surface sampling approaches, for example). It represents the first order ensemble average that models must agree with before they can hope to be validated using more detailed aerosol characterizations. Passive and active ground-based remote sensing can provide a complementarity as well as redundancy of information that enables the extraction of nearly all essential and robust aerosol parameters that influence the local radiative transfer budget

AboEl-Fetouh et al. (2020) present the most recent overview of ground-based, photometric remote sensing analyses across the Arctic. This overview includes a discussion of the ground-breaking multi-year AOD and Angstrom exponent seasonal climatology of Tomasi et al. (2015) across the

American, Canadian, European and Russian Arctic, Stone et al.'s (2014) 10-year AOD and Angstrom exponent climatology over Barrow, Alert (Ellesmere Island) and Ny Alesund (Svalbard), von Hardenberg et al.'s (2012) 6-year climatology that employed AERONET AODs, satellite retrievals and modelling over the Arctic, Breider et al.'s (2014) comparison of AERONET AODs and model-speciated extinction and absorption AODs, Xie et al,'s (2018) multi-year investigation over 8 Arctic sites of FMF and its relation to AOD, and Hesaraki et al.'s (2017) 4-year climatology of fine and coarse mode AODs over 5 stations in the North American Arctic. AboEl-Fetouh et al. (2020) present their own 8- to 17-year climatology of 6 AERONET stations across the North American and European Arctic[4] that included the seasonal variation of intensive and extensive parameters (PSD, fine and coarse mode AOD, fine and coarse mode effective radius and FMF).

With respect to the specific question of natural aerosols, nearly all of the papers on ground-based remote sensing discussed above reported on the springtime influence of Asian dust (either as a significant decrease in Angstrom exponent or significant increase in coarse mode AOD). AboEl_Fetouh et al. (2020) showed that the influence could be attributed to a small coarse mode peak at a radius of around 1.3 μm. Stone et al. (2014) reported on the likely coarse mode AOD influence (inferred from systematically small values of Angstrom exponent) of sea-salt aerosols at Barrow, Alaska. O'Neill et al., (2012) used sunphotometry, lidar measurements, satellite retrievals and HYSPLIT backtrajectory modelling to investigate stratospheric sulphate intrusions over Eureka due to the 2009 Sarychev volcanic eruption. In Paper 1 we employed ground-based sunphotometry, ground-based FTIR (Fourier Transform IR) retrievals, lidar profiles, satellite remote sensing and aerosol modelling (NAAPS) to analyze an extreme smoke event over Eureka driven by pyrocb (extreme convection) fires near Prince George, BC. In Paper 2 we reported on the unprecedented detection of a local dust plume (based solely on satellite retrievals) induced by drainage-flow along glacial-river basins produced by the cold-air dynamics of high elevation glaciers surrounding Lake Hazen (located in northern Ellesmere Island in the high-Arctic).

There are relatively few satellite-based, passive remote sensing analyses of Arctic aerosols over land because AOD retrievals in that region are problematic in general (as briefly described in Paper

[4] Contextualized by Breider-type, model-speciated, seasonal variations of coarse and fine mode AODs

2). On the other hand, the ultra-violet technique for retrieving the "aerosol index" (AI) can be readily employed over the Arctic because it is more sensitive to high altitude aerosols: Fromm et al. (2010) showed AI returns over high-Arctic landforms due to intense "pyroCB" fires in Alaska. Satellite-based, passive retrievals of AOD over Arctic water are relatively common but subject to the constraints of the short ice-free season. Satellite-based, active (Lidar) remote sensing retrievals over the Arctic are frequently reported in the literature: they are largely based on CALIOP (Cloud-Aerosol Lidar with Orthogonal Polarization) and, more recently, ALADIN (Atmospheric Laser Doppler Instrument) retrievals. Rose et al. (2003) employed MODIS (Moderate Resolution Imaging Spectroradiometer) IR imagery and TOMS AI imagery to study a Polar winter plume emanating from an Icelandic volcanic eruption. O'Neill et al. (2012) used satellite-based imagery (MODIS and OMI) and CALIOP profiles as well as ground-based measurements such as sunphotometer AODs, AHSRL (Arctic High Spectral Resolution Lidar) and CRL (CANDAC Rayleigh-Mie-Raman Lidar) profiles to investigate the effects of the 2009 Sarychev volcanic eruption over the Arctic. Tomasi et al. (2015) analyzed satellite-based MODIS, MISR (Multi-angle Imaging Spectroradiometer), and AATSR (Advanced Along Track Scanning Radiometer) AOD retrievals over large parts of the oceanic Polar Regions during the spring and summer. Di Pierro et al., (2013) used CALIOP to examine the vertical, horizontal and temporal variability of tropospheric aerosols in the Arctic regions during 2006–2012.

1.1.Project Objective

The original overarching objective of this research was to better understand the nature of natural aerosols in the Arctic. The identification and study of natural Arctic (Eureka) aerosols such as smoke, volcanic aerosols, dust, sea-salt and level Ib PSCs was a general objective of the proposed research project at the beginning. The ultimate goal was to characterize the optical and microphysical properties of a cross section of natural aerosols within the constraints of being able to capture specific events of opportunity over the last few years.

1.2.Hypothesis

The original general hyphothesis was that ground-based remote sensing data, supported by auxiliary information such as satellite-based remote sensing data, surface aerosol data, and model

simulations could be employed to adequately characterize and understand the properties of different natural aerosols in the high Arctic. By "adequately characterize" we mean't that the remote sensing retrieval analysis would demonstrate an acceptable level of accuracy and robustness (would not be limited by the uncertainties of the data) and it would exhibit physically defendable redundancy and correlation with other independent sources of information. We believe that we largely attained these goals within the context of Paper 1 and Paper 2 (with the added twist that we had to adapt to no ground-based remote sensing data in the case of Paper 2: the primary source of data was the satellite remote sensing data).

1.3. Choice of articles

While we investigated numerous natural aerosol events over the Arctic (see the Future work section below) we eventually focussed our article selection on two extraordinary events that were of more general interest. These two articles, paper 1 on the identification and characterization of an extreme high-Arctic smoke event over our PEARL (Eureka) observatory on Ellesmere Island and paper 2 on the identification and characterization of a drainage-flow (glacier-induced) dust plume over Lake Hazen (300 northeast of Eureka) are summarized below in the Conclusions section.

2. Paper 1: Extreme smoke event over the high Arctic

Keyvan Ranjbar[a1], Norm T. O'Neill[a], Erik Lutsch[b], Emily M. McCullough[c], Yasmin AboEl-Fetouh[a], Peng Xian[d], Kim Strong[b], Vitali E. Fioletov[e] Glen Lesins[c], Ihab Abboud[e]

[a] Centre d'Applications et de Recherches en Télédétection, Université de Sherbrooke , Sherbrooke, QC, Canada

[b] Department of Physics, University of Toronto, Toronto, ON, Canada

[c] Department of Physics and Atmospheric Science, Dalhousie University, Halifax, NS, Canada

[d] Atmospheric Properties and Effects Section, Naval Research Laboratory, Monterey, CA

[e] Environment and Climate Change Canada (ECCC), Toronto, ON, Canada

[1] Corresponding author E-mail address: Keyvan.ranjbar@usherbrooke.ca

Keywords: Extreme smoke event, high Arctic, aerosol optical depth (AOD), fine mode AOD

Supplementary data to this article can be found online at: https://doi.org/10.1016/j.atmosenv.2019.117002

Abstract

The intense western Canadian fires of August 2017 resulted in extreme, high-Arctic fine mode (FM) smoke AODs (aerosol optical depths) over a 2008 to 2017 (10-year) sampling period. The primary measurements employed to monitor smoke events were FM AODs derived from the measured AOD spectra of two AEROCAN / AERONET (CIMEL) sunphotometers at Eureka, Nunavut, Canada. The FM AOD attribution is argued to be a necessary condition for the presence of smoke. Various supporting information, including the correlation with smoke proxy (CO) retrievals, the high frequency (rapid diurnal variation) and the high amplitude nature of the FM AODs, ground-based backscatter lidar profiles, the redundancy of the double CIMEL retrievals, satellite remote sensing, aerosol modeling and backtrajectories indicated that the peak event was likely due to smoke from extreme pyroCb fires in British Columbia.

The hypothesis that the FM AOD peak event was an extreme event was tested for a derived ensemble of fine mode events and their peaks over the 10-year sampling period. The results confirmed the hypothesis at the 0.001 level of significance. Important indicators that the 10-year ensemble of FM AOD events did indeed represent smoke were their high frequency and high amplitude FM nature, their occurrence during the Boreal forest fire and agricultural fire seasons in Canada and Asia, and their strong correlation with CO abundances retrieved from FTIR measurements (when sufficient FM AOD and CO statistics were available).

In the process of accumulating climatological-scale, monthly-binned fine mode AOD statistics, we found moderate correlations with forest fire or agricultural fire emissions from the Boreal North American, Boreal Asia or Central Asia regions as well as with CO retrievals at Eureka. We argued that confounding factors constraining the monthly binned fine mode AOD vs emissions correlations were associated with the monthly-binned meteorological dynamics (with notable, event-level, exceptions) while confounding factors constraining fine mode AOD vs CO correlations included the different physio-optical nature of those smoke proxies (solar attenuation by fine mode particle scattering versus solar attenuation by molecular absorption). We also employed historic (2005-2010) AHSRL (Arctic High Spectral Resolution Lidar) profiles to estimate an optically averaged smoke plume height of ~ 3 to 3 ½ km during the spring and summer seasons.

1. Introduction

1.1. General considerations

The literature is replete with the observation and analysis of extreme events associated with GHG-driven increases in atmospheric thermal energy (see, for example, IPCC, 2013). A manifestation of extreme events, peculiar to the Boreal forest regions of the world, is the apparent increase in the frequency and strength of Boreal forest fires (see the following section for details). The occurrence of extreme smoke events over the high Arctic would be an important consequence of the extreme forest fire events. In recent years we have witnessed an apparent increase in the occurrence and severity of smoke events at Boreal forest latitudes and quite plausibly in the radiative impacts (both direct and indirect) of those events. Boreal forest smoke frequently finds its way to the high Arctic (see Saha et al., 2010, for example) and so one would expect a parallel increase in extreme smoke events. The precariousness of Arctic climate change makes such a consideration of primary concern as a source of radiative forcing uncertainty in climate models.

A robust indicator of smoke intrusions over a given site is the columnar measurement of fine mode (FM) aerosol optical depth (AOD) at a particular wavelength. This necessary (but not sufficient) evidence for a smoke event, variously supported by lidar backscatter and depolarization profiles, trace-gas measurements of gaseous smoke products (such as CO), satellite-based radiance and AOD imagery, satellite-based fire emissions imagery, back trajectories, and aerosol modelling yields high confidence in predictions of smoke presence (ibid). Over the high Arctic, a (relatively sudden) diurnal increase in FM AOD is, according to our experience, usually associated with smoke intrusions but can also be induced by high-frequency volcanic or pollution (sulphate-dominated) events of southern origin (illustrations are, respectively, the Kasatochi and Sarychev volcanic plume events described below and the early spring and autumn, Asian pollution-layer events reported by Di Pierro et al., 2011).

1.2. Climatological background for smoke reaching the North American high-Arctic

1.2.1. Forest fire emissions that impact the high Arctic

Biomass burning emissions that would significantly affect smoke measurements in the high Arctic are largely limited to the three vast regions defined by the authors of the GFED (Global Fire Emissions Database): these are the Boreal North America (BONA), Boreal Asia (BOAS) and

Central Asia (CEAS) regions (van der Werf et al., 2006). The dominant class, in terms of biomass burning emissions in the BONA and BOAS regions is the Boreal forest, while agricultural lands are the dominant class in the CEAS region (ibid).

Soja et al. (2007) observed that positive, burnt-area trends existed for Canada (1920 – 2006), Alaska (1950 – 2006) and Russia (1980 – 2006) "although the statistical relationships are not strong" (R^2 values vs time were < 0.18 for all three regions from 1950 to 2005). More generally they make an argument for the greater frequency of severe events with, for example, an affirmation that "5 of the 8 largest fire years transpired in the last 17 yr (1989-2005)" in the case of the Canadian database. van der Werf (2017) presented annual (1997 to 2016) estimates of fire carbon emissions: one concludes (from their Figure 9 results) that there were marginally significant emissions increases for the Boreal forest in the BONA region (correlation coefficient of 0.4) and no discernable trend for the Boreal forest in the BOAS region. Agricultural fires in the CEAS region also showed no discernable trend. What is evident in their BONA and BOAS temporal plots is the intermittent nature of annual emissions with extreme years occurring around every 4-6 years. In contrast to these marginally significant increases in pan-continental emissions, one finds reports of longer fire seasons in Canada and the U.S. (Schoennagel et al., 2017) and claims of significantly greater large-fire frequency and areas burned in Canada (NRCAN, 2016).

1.2.2. Tropospheric flow climatology and its impact on smoke intrusions into the high Arctic

Climatology reveals that the lower tropospheric flow during July and August is favourable for the transport of aerosols from the the BONA region into the Canadian high Arctic: NCEP/NCAR reanalysis averaged from 2007 to 2017 shows a trough axis in the geopotential heights at 700 and 500 hPa extending south from a low near the North Pole into the central portions of the Asian continent (see S1 and S2 of the Supplementary material). This configuration (what we will call the "Asian trough") allows the geostrophic wind to have a northward component downstream (east) of the trough: that component generally facilitates transport into the Canadian Arctic. The presence of an Alaskan trough may shift this region of transport to the Arctic further to the east.

1.2.3. Long term trends in smoke AOD

There are numerous sunphotometry articles on the observation of smoke events over the North American and European Arctic (see, for example, Stohl et al. (2006) on the multi-station AOD analysis of Arctic smoke induced by the 2004 Boreal forest fires, Warneke et al. (2010) on spring-2008 (ARCTAS) smoke events due to agricultural fires in southern Russia, O'Neill et al. (2008) on the observation of weak smoke events over Eureka in 2007, Myhre et al. (2007), Markowicz et al. (2016) on smoke observations over the European Arctic (Svalbard) associated with, respectively, European agricultural fires and western North American Boreal forest fires). A sampling of Arctic-AOD climatologies, for which smoke was an important analysis component, includes the Alaskan studies of Eck et al. (2009) as well as the more Arctic-scale studies of von Hardenberg et al. (2012), Stone et al. (2014), Breider et al. (2014), Hesaraki et al. (2017), and a notable series of climatological-scale papers that culminated in the "historical overview" of Tomasi et al. (2015). While particular severe years in terms of smoke AOD were noted in these studies, none showed a long term tendency of increasing smoke AOD. In fact the most prevelant trend noted was a decrease in [fine mode] AOD that was ascribed to decreases in anthropogenic SO_2 emissions from Russia and Europe (Tomasi et al., 2012).

1.2.4. Altitude of smoke events over the Arctic

A commonly accepted paradigm for understanding the dynamics of particle transport into the Arctic is that the Arctic or polar dome forces air parcels of southern origin to be transported to the mid to upper Arctic troposphere along isentropic pathways (see, for example, Stohl et al. (2006) and Law and Stohl (2007)). This principle, combined with the smoke source dynamics of pyro-convection events associated with fire activity (see, for example Damoah et al. (2006)) provide a strong argument for optically significant smoke (often in the form of distinguishable smoke plumes) being largely transported to the mid or upper troposphere. Empirical, event-level evidence for this resides in various studies involving co-located lidar and photometric measurements (see for example, O'Neill et al. (2008) and Saha et al. (2010)) and/or modelling simulations supported by auxilliary data (Stohl et al., 2006).

These qualitative arguments aside, we are not aware of any study in the literature which attempted to characterize average smoke plume height in the high Arctic across climatological-scale time periods. Thus, in order to support our abovementioned climatologies concerning the average

tropospheric flow of smoke into the Arctic, we performed our own assessment of average smoke plume height. A multi-year (2005-2010) analysis of the AHSRL lidar data at Eureka indicated an optically averaged smoke plume height ~ 3 ½ km during the summer Boreal forest fire season, ~ 3 km during the spring and 1-2 km during the fall (c.f. O'Neill et al.,2008. for a discussion of the AHSRL in the context of AOD measurements and S3 of the Supplementary material for a graphical illustration of the smoke plume classification approach and a brief discussion of the classification process, as well as the height computation technique). Similar computations were carried out using the results of Tomasi et al. (2015) who analyzed a year's worth of lidar data over the European high Arctic site of Ny Alesund, Svalbard (1 November 2012 to 31 October 2013): using their backscatter optical depth computations, we derived optically averaged aerosol plume heights of ~ 3 km for all months between April and September (see S4 for the final year to year results for both Eureka and Ny Alesund). Both sets of results are not inconsistent with the 1985-1990, 1996-2004, SAGE II, 1.02 μm extinction coefficient profile climatology of Treffeisen et al. (2006) which suggests optically weighted altitude means ~ 3 km between March and September across a latitude band of 60 – 80°N (the conditional nature of our affirmation derives from the fact that the SAGE II extinction coefficient profiles were limited to a lower altitude minimum of ~ 2 km) The spring and summer, optically-averaged altitude of ~ 3 km for Eureka and Ny Alesund correspond to a pressure altitude ~ 700 mb (i.e close to the 700 mb standard employed above to characterize average tropospheric flow climatologies).

1.3. Objectives of this paper

In this communication we seek to investigate, using ground-based AOD measurements and supporting data, a very strong smoke event that occurred over the Eureka observatory in August of 2017. This investigation will necessarily look at the high-frequency level (individual AOD retrievals) to characterize the nature of the August 2017 event as well as across a multi-year sampling period (MYSP) from 2008 to 2017 in an attempt to characterize the climatological-scale, event-level statistics of all smoke events. We also investigate monthly-binned statistics across the MYSP in order to achieve a low frequency climatology that contextualizes the higher-frequency results.

2. Site, instrumentation and retrieval techniques

Our study focusses on measurements acquired at the high-Arctic, Polar Environment Atmospheric Research Laboratory (PEARL) in Eureka, Nunavut, Canada. PEARL includes two labs separated by a distance of 15 km : the 0PAL (0-altitude PEARL Auxiliary Laboratory) at near sea-level elevation (10 m) and the Ridge Lab[5] at 610 m elevation (coordinates 79° 59' 24" N, 85° 56' 20" W, and 80° 03' 14" N, 86° 25' 01" W respectively). The Ridge Lab hosts an AEROCAN / AERONET CIMEL sunphotometer / sky radiometer along with a Bruker IFS 125HR Fourier Transform Infrared (FTIR) spectrometer (see O'Neill et al. (2008) and Viatte et al. (2014) respectively for details on these instruments). The 0PAL lab hosts a 2nd CIMEL instrument co-located with the CANDAC [6] Rayleigh-Mie-Raman Lidar (CRL). 0PAL also hosted the abovementioned AHSRL.

AERONET provides two types of data products and retrievals : (i) spectral extinction and sky (almucantar) radiance measurement from which microphysical and optical parameters at a relatively low frequency (once per hour in clear-sky conditions) are retrieved using the Dubovik inversion (Dubovik and King, 2000) and (ii) only spectral extinction measurements from which a more limited set of microphysical and optical parameters are retrieved at a significantly higher frequency (once every 3 minutes in clear-sky conditions) using the SDA algorithm of O'Neill et al. (2003). Both retrieval types provide fine-mode (FM), coarse-mode (CM) and total AOD as a standard output product (the SDA products are labelled τ_f, τ_c and τ_a respectively and are taken at a reference wavelength of 500 nm). The τ_f and τ_c division is often a means of segregating different species of aerosols (Hesaraki et al., 2017) and of effectively performing spectral cloud screening by separating fine mode aerosols from coarse mode cloud (see Baibakov et al. (2015) and O'Neill et al. (2016), for example). For the purposes of this paper, we chose to employ the high-frequency SDA retrievals in order to better understand the detailed dynamics of the August

[5] We should note that there is a degree of confusion about the label "PEARL" : it is mean't to represent the complex of (three) atmospheric labs at Eureka (0PAL, the Ridge Lab and the flux tower at "SAFIRE") but AERONET uses the label "PEARL" to represent the Ridge Lab CIMEL. In this paper we will refer to the Ridge Lab CIMEL and will employ PEARL in its established multi-lab usage

[6] Canadian Network for the Detection of Atmospheric Change

2017 event (supported by the high-frequency CRL profiles) and because the relatively low-frequency retrievals of the Dubovik inversion tend to dampen out high-frequency / high amplitude smoke-AOD excursions due to the per-hour sampling limitations. We also chose to employ the Level 1.0, version 3 SDA retrievals to minimize the filtering out of legitimate smoke AODs (Eck et al. (2018) present some examples of this type of omission error).

2.1. τ_f measurements at 0PAL and the Ridge Lab

Variations in τ_f are a well-known signature of smoke aerosols (see, for example, Eck et al., 2009). In general, we have found both FM and CM events to be consistently coherent with synchronous, high-frequency lidar profiles of backscatter coefficient and depolarization ratio (see, for example, O'Neill et al. (2008) for sunphotometry and Baibakov et al. (2015) for starphotometry). The relatively short distance between 0PAL and the Ridge Lab means that τ_f retrievals at the two facilities provide a high degree of optical redundancy which we often exploit to verify the opto-physical fidelity and robustness of measured AOD spectra and the resulting SDA retrievals (see, for example, Hesaraki et al. (2017) for illustrations of this notion of robustness).

2.2. CO measurements at the Ridge Lab and their link to τ_f variation

The FTIR spectrometer at Eureka provides total column measurements of gaseous products known to be tracers of biomass burning (Viatte et al., 2013, 2014, 2015; Lutsch et al., 2016). In the context of τ_f retrievals, a columnar smoke product such as CO (units of mol.-cm^{-2} ÷ 10^{18}) provides supporting information that can help confirm the presence of smoke aerosols in the high Arctic (Viatte et al., 2014, 2015). However, its fundamental optical mechanism is absorption while the fundamental optical mechanism of τ_f is scattering by (largely) sulphate and / or organic carbon (OC)[7] FM aerosols : the τ_f and CO retrieval products are themselves influenced by a complex mixture of natural and anthropogenic emission sources and the physical / chemical interactions undergone between the source and the high Arctic. While they both generally correlate with a high-frequency intrusion of smoke they are subject to secondary removal mechanisms (beyond the

[7] See, for example, Figure 9 of Breider et al. (2014) for simulations showing seasonal dynamics of total and absorbing AOD across a number of Arctic stations (where the small amplitude of the latter indicates a dominance of scattering AOD).

primary forces of advection) : CO, for example, is removed via OH chemistry driven by the springtime onset of solar radiation. In the end, the covariation (and notably the high frequency covariation) of CO and τ_f represents added support for the identification of a significant smoke event but, by itself, is not a sufficient condition for its identification.

3. The August 2017 event and its multi-year context

3.1.Characterization of the event

Figure 1 shows the very strong τ_f amplitudes at the Ridge Lab and 0PAL sites during the August 2017 smoke event. The τ_f peak value on 19 August 2017 is nearly two orders of magnitude larger than the "clear-day" value of ~ 0.02 reported in O'Neill et al. (2008). Figure 1 also shows (light pink diamonds) the smoke AOD simulated by the NAAPS[8] model (Lynch, et al., 2016) at a temporal resolution of 6 hours (more details on this diagnostic run are reported on the S11 slide of the supplementary material).

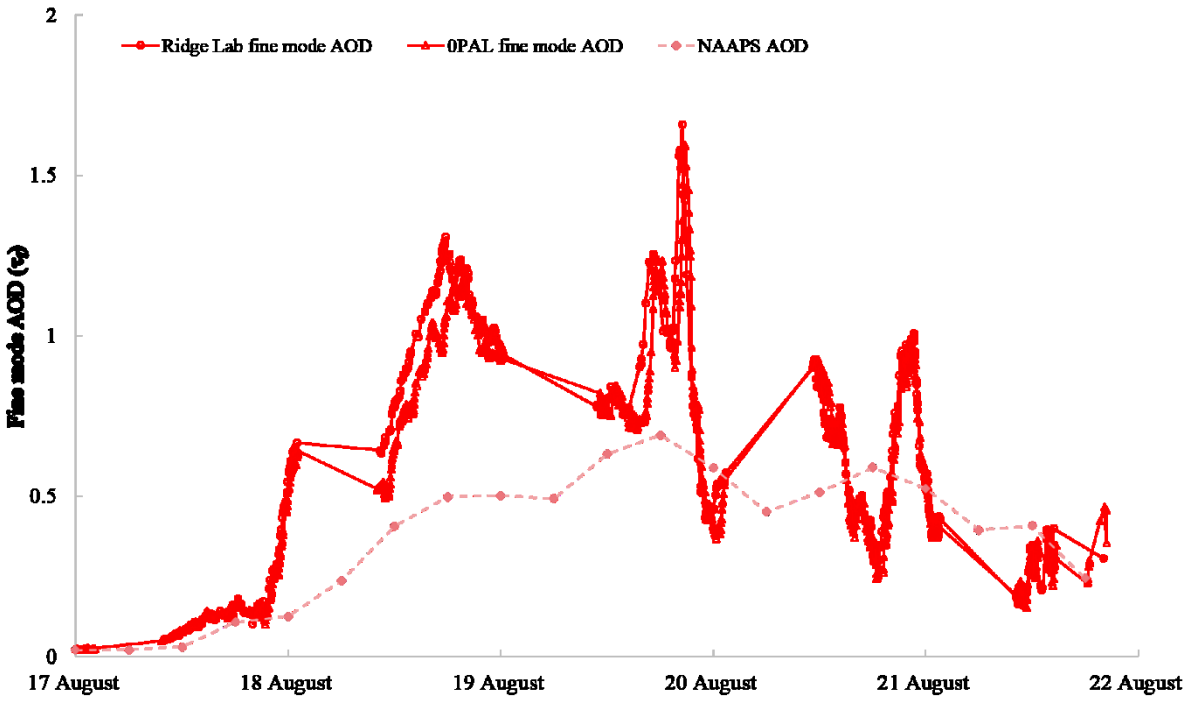

Figure *1* : τ_f variation at Ridge Lab and 0PAL during the 5-day duration of the August, 2017 event. The tic marks above the date labels correspond to 00:00 UTC. The pinkish dashed line represents simulations of

[8] Navy Aerosol Analysis and Prediction System (Naval Research Laboratory (NRL) in Monterey, CA)

the smoke AOD from the NAAPS diagnostic run (6 hour temporal resolution and 1° x 1° spatial resolution ; see the S11 caption for more details on this run)

Figure 2 shows a composite of key data employed in the identification and characterization of the 19 August peak (τ_f retrievals at 0PAL and the Ridge lab, the CRL backscatter profile, the NAAPS smoke mass concentration profile from the NAAPS diagnostic run and the MODIS-Terra image acquired near the time of the τ_f peak). The supplementary material (S7 to S12) provides supporting graphics and discussion details related to Figure 2 (including a brief discussion of the west to east lag in the τ_f plots of S7 and S8, between the Ridge Lab and 0PAL CIMELs). These details, which also include MISR imagery as well as stereoscopic plume height retrievals and HYSPLIT[9] backtrajectories indicate that the 19 August smoke peak (corresponding to a plume around 7 km altitude at the time of the 20:40 UTC 0PAL peak) likely originated from forest fire emissions in western Canada. The HYSPLIT backtrajectories were however, less than conclusive given the type of divergence seen in the plume origins coupled with the complexity of the backtrajectories prior to their leaving the Canadian Arctic mainland (c.f. S10 and its caption).

Forest fire activity was particularly notable in south central British Columbia (BC) (as suggested by the hotspot clustering in S10) where biomass burning emissions near Prince George BC were judged to be so intense that the period from 13 to 15 August produced stratospheric smoke with unprecedentedly strong Aerosol Index (AI) values (Fromm et al., 2018; Peterson et al., 2018). We believe that the origin of the (Figure 2 and S8) 7 km plume was likely the extreme BC fires from mid to upper tropspheric injections of smoke as suggested by the S10 (blue) backtrajectory. At the same time, there was a concentration of fire sources southeast of Great Slave Lake (S10) which probably contributed to the strong (Figure 2 and S8) plumes seen around 4 km on 19 August (rather than the 7 km plume as suggested by the red colored backtrajectory of S10, if one were to assume high altitude emissions for the Great Slave Lake fires). In order to support these hypotheses, we simulated high altitude emissions at Prince George (the NAAPS diagnostic run) and obtained a decreasing altitude plume (~ 10 down to 8½ km) on 19 August (details in the caption of S11). A control run where all emissions were assumed to be near the surface produced the results of S12 : a plume with a mean height ~ 3 km. Putting aside the non negligible differences in detail of the

[9] HYbrid Single-Particle Lagrangian Integrated Trajectory

real and simulated higher altitude plumes (which we believe could be improved upon with better vertical profile knowledge of the high altitude Prince George emissions) we then make the argument that the pyroCb emissions of Prince George are the likely source of the extreme 19 August smoke event at Eureka.

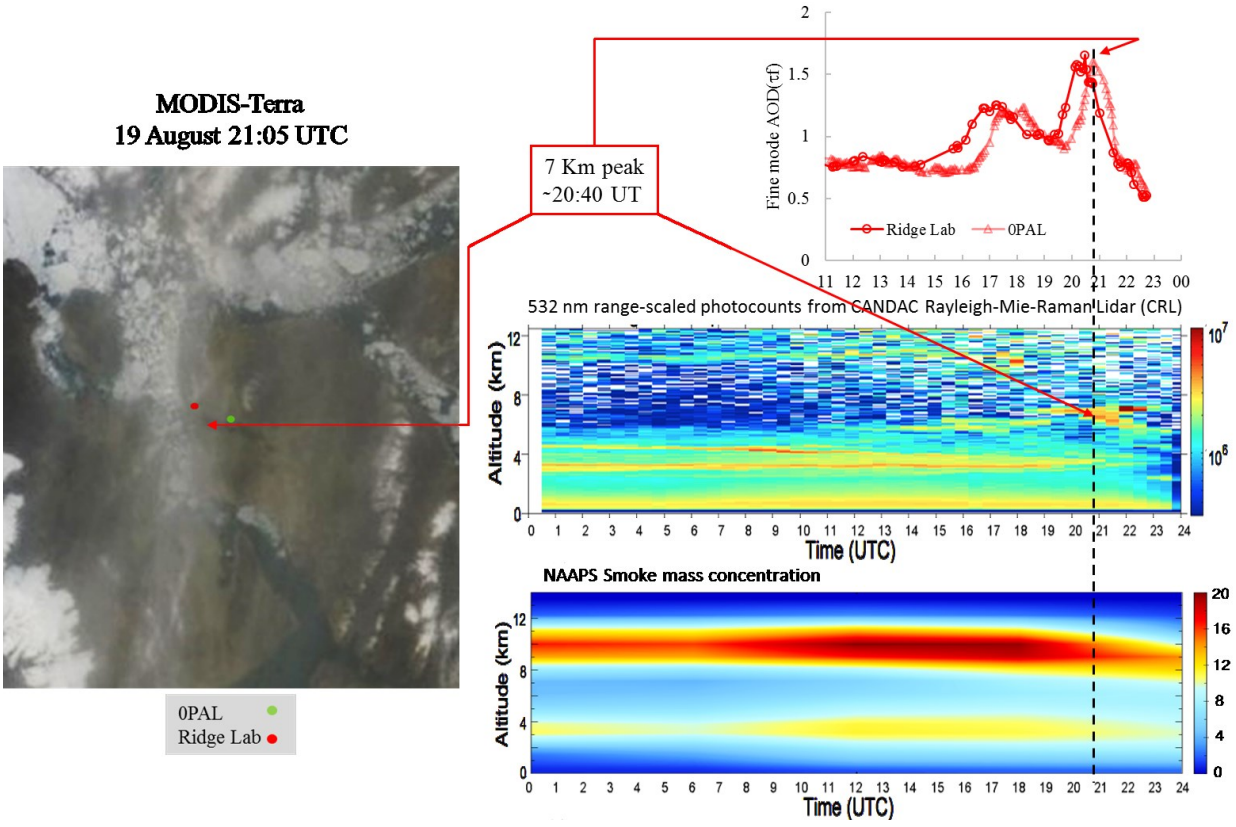

Figure *2* : The 19 August 2017 extreme smoke event over Eureka. Clockwise; the MODIS-Terra image at about the time of the fine mode AOD peak over 0PAL, the temporal variation of the Ridge Lab and 0PAL fine mode AODs, the CRL range corrected photon counts and the NAAPS smoke concentration ($\mu g/m^3$) profile. See the caption of S11 for more details

The month of August 2017 was, in effect, a meteorological departure from the climatological means discussed above. The Alaskan geopotential troughs at 500 and 700 hPa had a larger amplitude compared to the S2 climatology and, to a degree, dominated over the Asian trough (c.f. S15 and S16 of the Supplementary material for the averaged GFED emissions and the averaged meteorology during August 2017). In general this allowed aerosols released by fires in western Canada to be advected nearly directly to the Canadian high Arctic. We should remind the reader that, at the event level, such climatological affirmations are the norm and not the rule : for example,

there was apparent advection events from BOAS fires that passed over Eureka on 12 and 13 August (c.f. the NAAPS smoke-AOD simulations of video1 of the Supplementary material) that were not captured by the Eureka CIMELS on 12[10] August but appeared to be captured, as a moderate τ_f variation, on 13 August.

3.2. FM AOD : multi-year comparisons with emissions

Figure 3a shows the variation of monthly averaged emissions from the BONA, BOAS and CEAS regions superimposed on $<\tau_f>$ (monthly mean) variation. Various features of interest are indicated directly on the graph. The August 2017 event can be seen to the right (the large $<\tau_f>$ peak being cut off to better appreciate the weak, more subtle $<\tau_f>$ variations during the other years). The fine mode stratospheric sulphates of the Kasatochi and Sarychev volcanos of 2008 and 2009 act as confounders of the correlation between emissions and $<\tau_f>$. The "low duty cycle" label points to examples of $<\tau_f>$ values whose representativeness (relative to emissions that are not, for example, subject to being cutoff by the presence of clouds) is questionable for any given month (a low duty cycle being characterized as the occurrence of τ_f retrievals on 25% or less of the days in a given month).

Figure 3b shows the resulting variations with the removal of the volcanic sulphate contributions and the low duty cycle values. On this graph we have indicated the clear-day minimum from O'Neill et al. (2008) as a baseline at a τ_f value of about 0.02 (which we have renamed "clear-sky minimum"). The removal of the volcanic contributions, using estimates of volcanic $<\tau_f>$ from calculations similar to O'Neill et al. (2012), as well as a residual element of Kasatochi in 2009 as per Sioris et al. (2010), yielded significantly better correlations with the strong BOAS emissions in 2008. There was no significant correlation improvement with the weak emissions of 2009 while there was arguably an amplitude improvement in terms of what appears to be anomalously high $<\tau_f>$ values relative to the stronger emitting years of 2008 and 2010 (an "amplitude improvement" driven by the correction of the "Kasatochi residual" of Figure 3a). The removal of low duty cycle

[10] There were simply no measurements acquired on that date: a condition that usually results from the automated disabling of the instruments during thick cloud or precipitation events.

points typically had little impact except for a significant improvement relative to BOAS and BONA emissions in 2011.

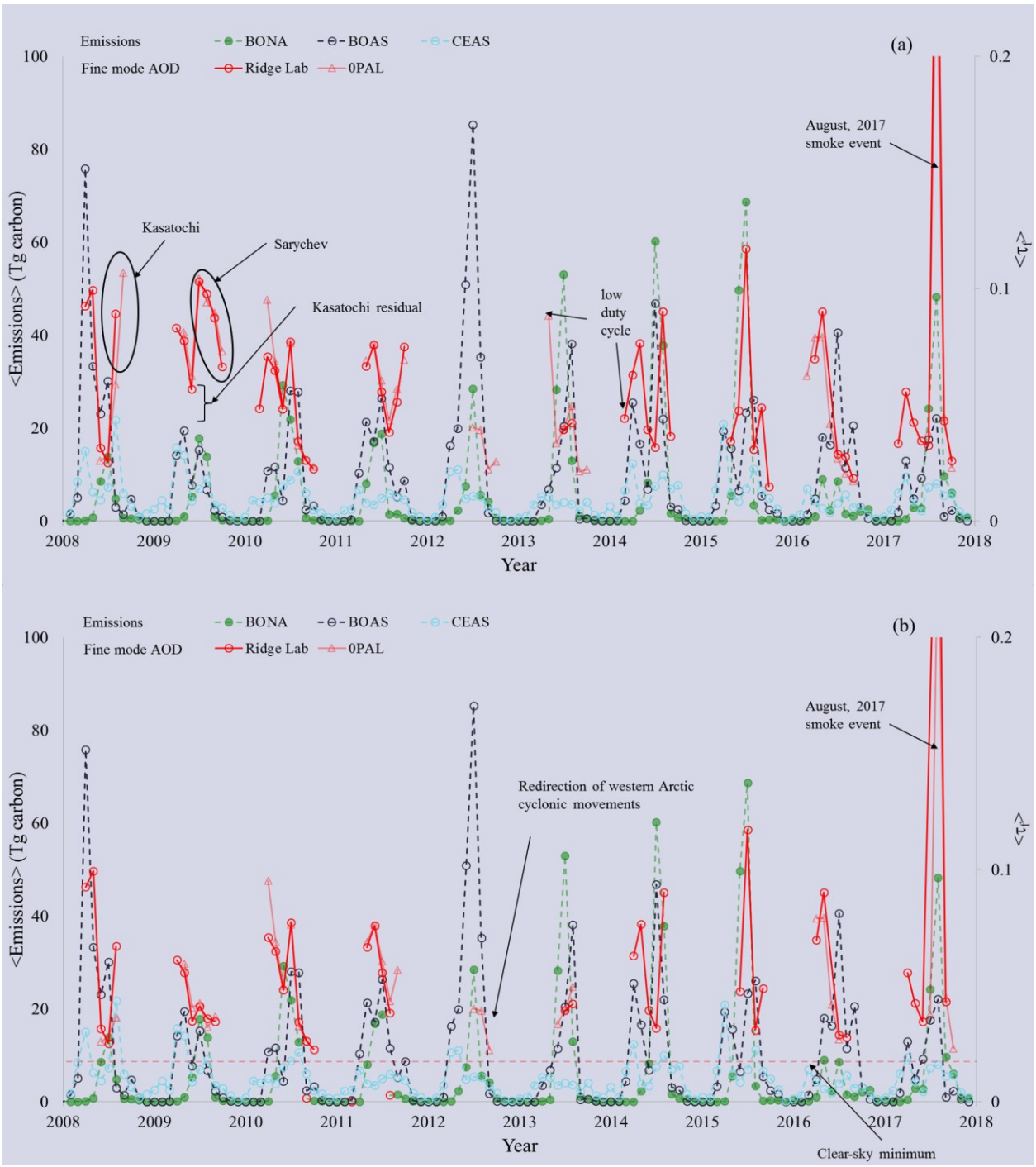

Figure 3 : (a) Right hand axis : $<\tau_f>$ (monthly average) variation at the Ridge Lab and 0PAL. Left hand axis : fire emissions for 3 GFED regions (BONA: Boreal North America, BOAS: Boreal Asia, CEAS: Central

Asia). There were no Ridge Lab retrievals and only 4 months of $<\tau_f>$ retrievals in 2012 because the Eureka facilities were, due to funding problems, being maintained by a skeleton staff. (b) caption is identical to the first two sentences of the Figure 3a caption. The volcanic contributions and the low duty cycle have been removed from the $<\tau_f>$ values. The duty cycle threshold was taken to be 25% ($<\tau_f>$ values with duty cycles less than 25% were eliminated)

Strong emissions in any given sector are no guarantee of strong $<\tau_f>$ variations at a distant Arctic site since the governing meteorology may not favour movement of smoke plumes over Eureka. The July 2012 meteorological dynamics are a case in point. The BOAS July emissions were at a 10-year maximum for the whole MYSP while 0PAL $<\tau_f>$ values were weak. NAAPS model simulations (video2) showed what amounted to an apparent systematic redirection of strong cyclonic movements of smoke AOD (coming from the general BOAS region) away from the Eureka region.

During July 2012 the 500 and 700 hPa winds were nearly zonal (a nearly straight west to east flow) over northern Asia. The absence of the climatological summer trough during that particular month (the Asian trough discussed above) allowed aerosols from the strong BOAS fires (c.f. S13 of the supplementary material) to be advected eastward, ending up over the North Pacific and unable to reach the Canadian high Arctic (c.f. S14 of the Supplementary material). The (video2) NAAPS animation shows visually how this meteorology facilitated flow towards the east and largely inhibited smoke-access to Eureka. The same animation indicates that, while the Alaskan trough may have facilitated some movement into the Arctic, it was largely ineffective in advecting smoke from the principle BONA sources (largely confined to a south-easterly band from the region of Great Slave Lake in the Northwest territories to Lake Winnipeg in the province of Manitoba, c.f. S13 of the supplementary material).

The fact that our solar sampling season at Eureka limits our analysis to roughly the months between April and September has no strong impact on any smoke-related, emission conclusions that we might draw (from results like those of Figure 3) because the significant biomass burning season in the BONA, BOAS and CEAS regions are largely coherent with the AEROCAN/AERONET sampling period. The supplementary material (S5) shows the integrated emissions over the 2008-2017 period : the stronger BONA and BOAS emission influences on τ_f and $<\tau_f>$ variability are

97% and 95% encompassed by that period while the weaker CEAS influences are 74% encompassed.

3.3. FM AOD - multi-year comparisons with CO retrievals

Figure 4a shows a (post-volcanic-corrected) multi-year comparison of $<\tau_f>$ and <CO> (monthly averages of CO total columns) at Eureka, while Figure 4b shows the variation of the $<\tau_f>$ vs <CO> correlation coefficients (R) over each year. In this case, we did not apply a low-duty-cycle correction to the retrievals since, by and large, the sun-tracking CIMELs and the FTIR spectrometer suffer very similar line-of-sight constraints (an obvious illustration being that the CIMELs and the FTIR automatically limit their acquisition of data when clouds contaminate the solar-pointing field-of-view). The corrections for volcanic intrusions provided a moderate increase in the Ridge Lab and 0PAL R value for 2008 and a strong R increase in 2009 for the Ridge Lab (0PAL, with its limitation to four summer months yielded a strong negative correlation with and without volcanic corrections).

Figure 4 : (a) Right hand axis : $<\tau_f>$ (monthly average) variation at the Ridge Lab and 0PAL (corrected for volcanic contributions). Left hand axis : <CO> total column. (b) Correlation coefficients for $<\tau_f>$ and <CO>

of Figure (a). The 2008 0PAL correlation coefficient (with its obvious negative correlation) was excluded to keep the R axis between 0 and 1.

In general, with the exception of 2010 for the Ridge Lab and 2008 for 0PAL, the correlation coefficients for each year were > 0.6 while the correlation for the total MYSP was greater than 0.5 for the Ridge Lab and 0.6 for 0PAL. These marginal R values speak to the above-mentioned complexity of comparing τ_f and CO retrievals (most notably, the relative strength of solar-chemistry-driven springtime <CO> decrease is not apparent in the $<\tau_f>$ variations). Changing the time bins from months to days to hours to minutes[11] is a not particularly fruitful exercise for weak correations that are affected by multiple influences. These influences include the impact of increasing the number of bins for weakly correlated points : if the larger-bin points are reasonably representative, then there is no reason to expect a significant increase in R (there is however reason to expect greater uncertainty in R if the number of larger bins is very small as, for example, in the extreme cases of 2012, 2013 and 2017 with pairs of τ_f/CO-common bins yielding unit R values at 0PAL). A R-degrading influence is the "smoke duty cycle" of common τ_f and CO bins : if that duty cycle does not straddle a sufficiently large portion of the smoke season (as in the case of 0PAL in 2008, 2012 and 2013 and Ridge Lab in 2013) then R values will, in general, be weak (or, if large, very uncertain) for larger binned regressions.

Significantly stronger correlations are, not unexpectedly, observed at the high-frequency event (plume) level: Figures 5a to 4f exhibit strong correlations ($0.88 \leq R \leq 0.98$) between groups of individual τ_f and CO retrievals for specific diurnal events across the MYSP (the blue symbols represent the contribution of the coarse mode optical depth which is generally associated with the presence of clouds; see the introduction of Section 2). Figure 5g and 5h exhibit weak correlation that is likely associated with the presence of cloud (and, in the former case, an apparent lack of natural τ_f and CO variation : the degree of correlation is accordingly more susceptible to cloud contamination). It should be noted however that these high-frequency events (involving a commonality of at least one τ_f and one CO retrieval in a given 5 minute time bin to achieve at least 4 common time bins across the event) were relatively scarce. There were challenging

[11] for each bin size we searched for bins that contained at least one common τ_f and CO retrieval

sampling problems associated with the τ_f inter-measurement period (the peak of the histogram of inter-sample times was ~ 3 minutes for the total MYSP) and that of the CO retrievals (histogram peak of ~ 30 minutes for the total MYSP) and the fact that CO retrievals were more likely to be filtered out by the presence of cloud than the τ_f retrievals. Increasing the time bins associated with the correlation analysis from 5 to 15 to 30 or 60 minutes did not systematically increase the R values.

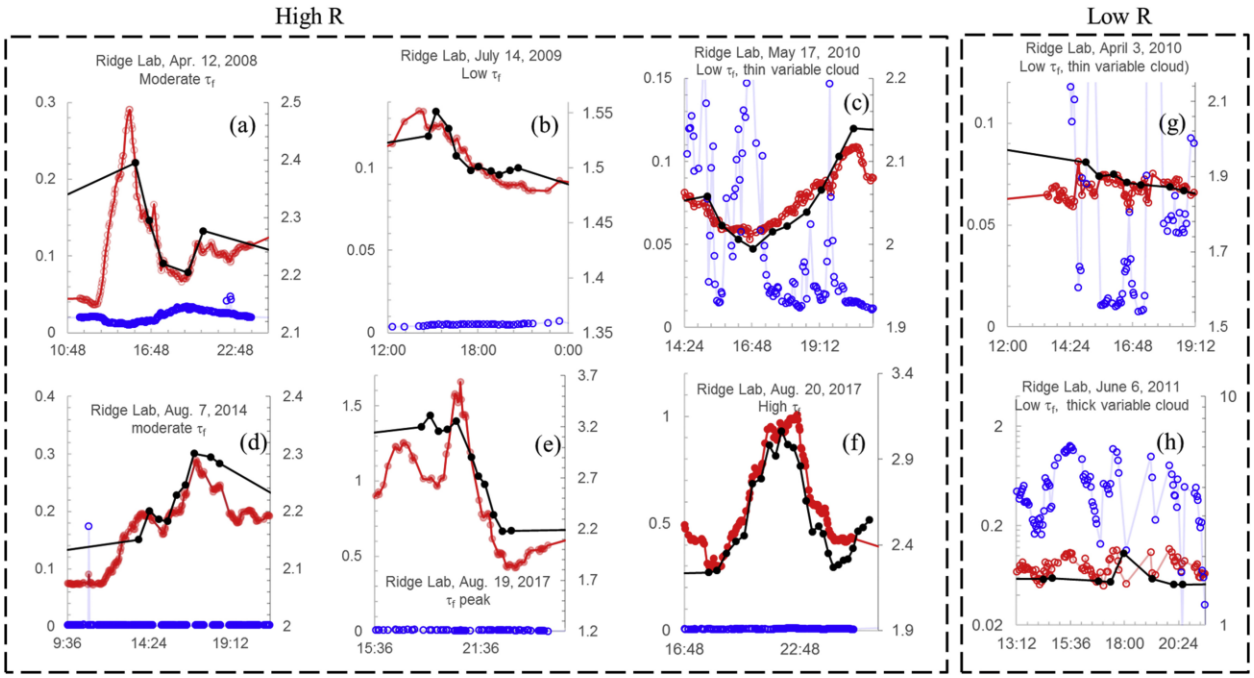

Figure 5 : Temporal variation of τ_f (red), CO (black) and τ_c (blue colored coarse mode optical depth). Graphs (a) to (f) ; high correlation coefficient in generally clear-sky conditions. Graph (c) shows that the τ_f retrieval appears to withstand the influence of cloud contamination while the FTIR generally avoided measurements in the presence of the thin cloud. "High R" refers to R values between 0.88 and 0.98 with time bins of 5 minutes. Graphs (g) and (h) ; low correlation ("low R") events that have been influenced by cloud contamination (the 3 April 2010 event actually yields negative correlation coefficients for larger time bins ~ hours).

3.4. The extreme nature of the August 2017 event

We chose our own variant of the peaks over threshold (POT) approach employed in extreme value theory to characterize extreme τ_f statistics across the MYSP (see, for example, Bezak et al. (2014) for a discussion of the POT approach). A peak was defined, according to the classical POT

method, as being greater than a threshold (taken to be $\tau_{f,thr} = 0.1$) but with a further constraint that it be part of a contiguous τ_f event (with at least six retrieval points) whose temporal profile began and ended with τ_f values below 0.1. This $\tau_{f,thr}$ choice is a compromise between physical reasoning of what constitutes a plume and achieving a statistically significant number of peak values (see also ibid for further discussion concerning this type of POT compromise). We believe that our POT constraints are more closely linked with the plume nature of smoke events and that they more readily avoid artifactual peaks that are the result of plume events being abruptly cut off by thick and rapidly varying cumulus-type clouds and/or continuous thin cloud optical depth (cirrus-type) contamination of the τ_f retrievals. The extraction of $\tau_{f,peak}$ values for all defined MYSP events yielded a total of 465 values for the combined case of the Ridge Lab and 0PAL. Fitting, as per ibid, a "Generalized Pareto distribution" (GPD) to the resulting histogram[12] yielded the best fit shown in the supplementary material (S6).

Figure 6 shows the variation of the annual peak τ_f values ($\tau_{f,peak}$) for the Ridge Lab and 0PAL. As previously indicated, the peak of 19 August 2017 represents the largest amplitude $\tau_{f,peak}$ value across the total MYSP. Given the POT processing and the resulting GPD fit, the estimated GPD probability of finding a larger, more extreme peak value is 0.09% (acceptance of the null hypothesis at a significance level of 0.001 for a p-value of 0.09% in standard statistical parlance) : alternatively stated we are 99.91 % sure that the 19 August 2017 peak can be viewed as a peak value given the MYSP statistics derived from the ensemble of τ_f retrievals). By contrast, the next larger $\tau_{f,peak}$ value (in 2014) can be associated with a GPD (p-value) probability of 0.34% (close to 4 times the 19 August probability of finding a larger, more extreme peak value). We also note that co-author Lutsch also reported on the extreme nature of the 17-22 August, 2017 event over Eureka in terms of FTIR measurements of NH3, CO, HCN, and C2H6 (Lutsch et al., 2019).

[12] Histogram normalized to yield a PDF approximation, to be precise.

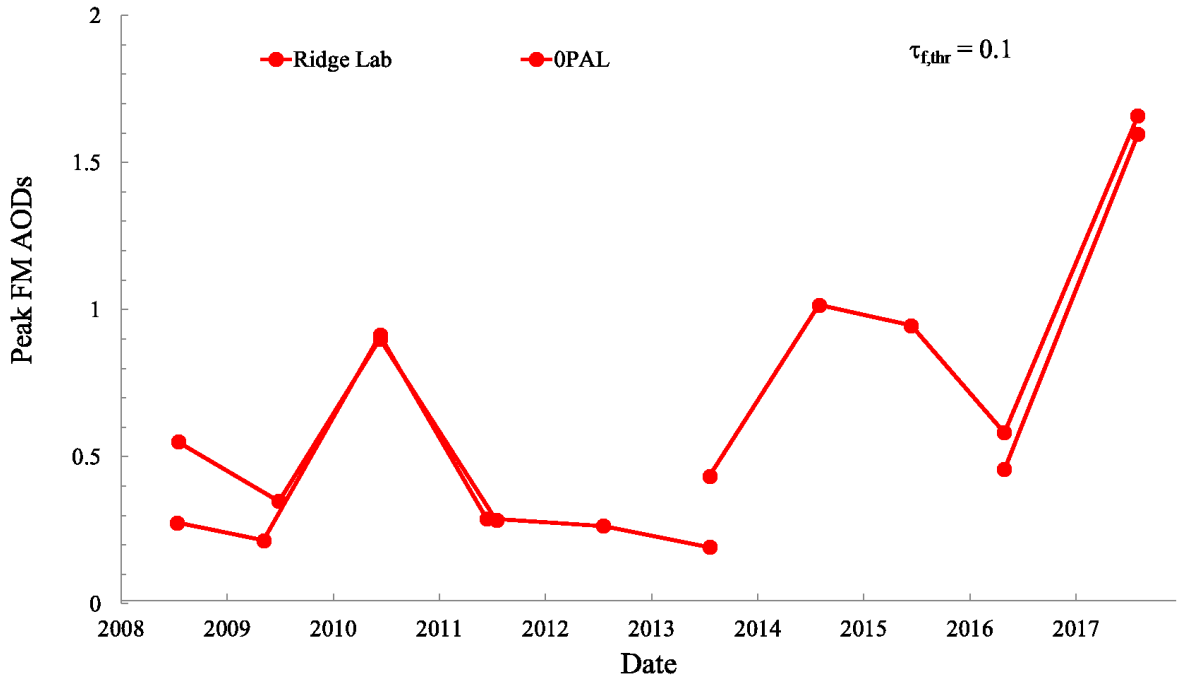

Figure 6： Peak FM AOD ($\tau_{f,pe\ ak}$) values for each year of our MYSP (the peaks are extracted from the fine mode events, defined using our variant of the POT approach ; see text for details).

4. Conclusions

The intense western Canadian fires of August 2017 resulted in extreme, high-Arctic fine mode (FM) smoke AODs (aerosol optical depths) over a 2008 to 2017 (10-year) sampling period. The primary high-Arctic measurements employed to monitor smoke events were acquired using two AEROCAN / AERONET (CIMEL) sunphotometers whose AOD spectra were transformed into FM AODs using the AERONET SDA algorithm. Our experience from the current and previous analyses indicate that the FM AOD attribution is a necessary condition for the presence of smoke.

Various supporting information, including the FM characterization, the correlation with smoke proxy (CO) retrievals, the high frequency (rapid diurnal variation) and high amplitude nature of the FM AODs, ground-based backscatter lidar profiles, the redundancy of the CIMEL retrievals (from two sites separated by 15 km and 600 m of altitude), MODIS radiance images, MISR profile retrievals, aerosol modeling and backtrajectories indicated that the peak event of 19 August 2017 was likely due to smoke from extreme pyroCb fires in British Columbia.

The hypothesis that the 19 August plume was an extreme event was tested using the peak over threshold approach to extract FM AOD peak statistics over the MYSP and fitting a Generalized Pareto Distribution to the resulting histogram-derived probability distribution functions. The (cumulative distribution function) derived from the GPD fit indicated that the 19 August plume was an extreme peak event at the 0.001 level of significance. Important indicators that the MYSP ensemble of FM AOD events that we chose for the POT approach did indeed represent smoke were their high-frequency (diurnally varying) and high-amplitude FM nature (all typical signatures of smoke), their occurrence during the Boreal forest fire and agricultural fire seasons in Canada and Asia, and their strong correlation with lower-frequency CO (smoke proxy) abundances retrieved from FTIR measurements (when those conditions allowed for a sufficient number of common FM AOD and CO retrievals to be acquired).

In the process of accumulating the MYSP climatological-scale, monthly-binned FM AOD statistics, we found moderate correlations with monthly-binned, forest fire or agricultural fire emissions from the Boreal North America, Boreal Asia or Central Asia regions (with better correlations when the 2008 and 2009 Kasotochi and Sarychev contributions were removed). Moderate correlations were also obtained with monthly-binned CO retrievals. We provided illustrations to support arguments that confounding factors constraining the monthly binned FM AOD vs emissions correlations were associated with the monthly-binned meteorological dynamics (with notable, event-level, exceptions) while confounding factors constraining FM AOD vs CO correlations included the different physio-optical nature of those smoke proxys (solar attenuation by FM particle scattering versus solar attenuation by molecular absorption). In part to support the relevant meteorological analyses, we employed historic (2005-2010) AHSRL Lidar profiles of backscatter coefficient and depolarization ratio to estimate an optically averaged smoke plume height of ~ 3 ½ km over Eureka during the summer Boreal forest fire season, ~ 3 km during the spring and 1-2 km during the fall.

5. Acknowledgements

We would like to acknowledge our gratitude for NSERC for CCAR funding via the PAHA project, the NSERC training program in Arctic Atmosphere Science as well as NSERC DG funding of Strong and O'Neill, the CSA, and the CFI for their financial support (the latter two for PEARL

support). The support of AEROCAN (Environment Change and Climate Change Canada), AERONET (NASA/GSFC), and the PEARL operations staff (led by Pierre Fogal) are gratefully acknowledged. We also wish to acknowledge the contribution of the AHSRL mentor (Ed Eloranta) for the profiles employed to generate S3 and S4.

6. Symbol and acronym glossary

AERONET	World-wide NASA network of combined sunphotometer / sky-scanning radiometers manufactured by CIMEL Éléctronique. See AERONET website for documentation and data downloads
AEROCAN	Federated Canadian subnetwork of AERONET run by Environment and Climate Change Canada (ECCC)
AHSRL	Arctic High Spectral Resolution Lidar
AOD	The community uses "AOD" to represent anything from nominal aerosol optical depth which hasn't been cloud-screened to the conceptual (theoretical) interpretation of aerosol optical depth. In this paper we use it in the latter sense and apply adjectives as required.
BOAS	Boreal Asia (defined by van der Werf et al., 2006).
BONA	Boreal North America (ibid)
CDF	Cumulative Distribution Function
CEAS	Central Asia (defined by van der Werf et al., 2006).
CO	Carbon monoxide (units of mol.-cm^{-2} ÷ 10^{18}). <CO> refers to the arithmetic mean
CRL	CANDAC Rayleigh-Mie-Raman Lidar
FTIR	Fourier Transform Infrared [spectrometer]
GPD	Generalized Pareto Distribution (de Zea Bermudez and Kotz, 2010)
HYSPLIT	HYbrid Single-Particle Lagrangian Integrated Trajectory
MYSP	Multi-Year Sampling Period (our 10-year period from 2008 to 2017)
MISR	Multi-angle Imaging SpectroRadiometer
MODIS	Moderate Resolution Imaging Spectroradiometer
NAAPS	Navy Aerosol Analysis and Prediction System (Naval Research Laboratory (NRL) in Monterey, CA)
0PAL	Zero altitude Polar Atmospheric Lab

PEARL	Polar Environment Atmospheric Research Lab (the name associated with the complex of 3 atmospheric labs at Eureka). In this paper we used "PEARL" in its proper multi-lab sense the Ridge Lab CIMEL to refer to the CIMEL at the Ridge Lab. AERONET uses the label "PEARL" to represent the Ridge Lab CIMEL
PDF	Probability Distribution Function
POT	Peak Over Threshold approach for extracting a population of event peaks (see, for e.g, Bezak et al., 2014)
R, R^2	Correlation coefficient, coefficient of determination
SDA	Spectral Deconvolution Algorithm described in O'Neill et al. (2003)
τ_x	τ_a, τ_f, *or* τ_c for total, fine and coarse mode AODs retrieved using the SDA algorithm at a reference wavelength of 500 nm. τ_a is conserved in the sense that $\tau_a = \tau_f + \tau_c$. This expression propagates into monthly averages.
$\langle\tau_x\rangle, \langle\mathrm{CO}\rangle$	Monthly arithmetic mean of individual τ_x, CO retrievals
x	x = *a, f, or c* (total, fine mode or coarse mode)

7. References

Baibakov, K., O'Neill, N.T., Ivanescu, L., Duck, T.J., Perro, C., Herber, A., Schulz, K.-H., Schrems, O., 2015. Synchronous polar winter starphotometry and lidar measurements at a High Arctic station. Atmos. Meas. Tech. 8, 3789–3809.

Bezak, N., Brilly, M., Šraj, M., 2014. Comparison between the peaks-over-threshold method and the annual maximum method for flood frequency analysis. Hydrol. Sci. J. 59, 959–977.

Breider, T.J., Mickley, L.J., Jacob, D.J., Wang, Q., Fisher, J.A., Chang, R.Y., Alexander, B., 2014. Annual distributions and sources of Arctic aerosol components, aerosol optical depth, and aerosol absorption. J. Geophys. Res. Atmos. 119, 4107–4124.

Damoah, R., Spichtinger, N., Servranckx, R., Fromm, M., Eloranta, E.W., Razenkov, I.A., James, P., Shulski, M., Forster, C., Stohl, A., 2006. A case study of pyro-convection using transport model and remote sensing data. Atmos. Chem. Phys. 6, 173–185.

de Zea Bermudez, P., Kotz, S., 2010. Parameter estimation of the generalized Pareto distribution—Part I. J. Stat. Plan. Inference 140, 1353–1373.

Di Pierro MD, Jaeglé L, Anderson TL. Satellite observations of aerosol transport from East Asia to the Arctic: three case studies. Atmospheric Chemistry and Physics. 2011 Mar 11;11(5):2225-43.

Dubovik, O., King, M.D., 2000. A flexible inversion algorithm for retrieval of aerosol optical

properties from Sun and sky radiance measurements. J. Geophys. Res. Atmos. 105, 20673–20696.

Eck, T.F., Holben, B.N., Reid, J.S., Sinyuk, A., Hyer, E.J., O'Neill, N.T., Shaw, G.E., Vande Castle, J.R., Chapin, F.S., Dubovik, O., 2009. Optical properties of boreal region biomass burning aerosols in central Alaska and seasonal variation of aerosol optical depth at an Arctic coastal site. J. Geophys. Res. Atmos. 114.

Eck, T.F., Holben, B.N., Reid, J.S., Xian, P., Giles, D.M., Sinyuk, A., Smirnov, A., Schafer, J.S., Slutsker, I., Kim, J., 2018. Observations of the Interaction and Transport of Fine Mode Aerosols With Cloud and/or Fog in Northeast Asia From Aerosol Robotic Network and Satellite Remote Sensing. J. Geophys. Res. Atmos. 123, 5560–5587.

Hesaraki, S., O'Neill, N.T., Lesins, G., Saha, A., Martin, R. V, Fioletov, V.E., Baibakov, K., Abboud, I., 2017. Comparisons of a Chemical Transport Model with a Four-Year (April to September) Analysis of Fine-and Coarse-Mode Aerosol Optical Depth Retrievals Over the Canadian Arctic. Atmosphere-Ocean 55, 213–229.

IPCC, 2013: Climate Change 2013: The Physical Science Basis. Contribution of Working Group I to the Fifth Assessment Report of the Intergovernmental Panel on Climate Change [Stocker, T.F., D. Qin, G.-K. Plattner, M. Tignor, S.K. Allen, J. Boschung, A. Nauels, Y. Xia, V. Bex and P.M. Midgley (eds.)]. Cambridge University Press, Cambridge, United Kingdom and New York, NY, USA, 1535 pp.

Law, K.S., Stohl, A., 2007. Arctic air pollution: Origins and impacts. Science (80-.). 315, 1537–1540.

Lutsch, E., Dammers, E., Conway, S., Strong, K., 2016. Long-range transport of NH3, CO, HCN, and C2H6 from the 2014 Canadian Wildfires. Geophys. Res. Lett. 43, 8286–8297.

Lutsch, E., Strong, K., Jones, D.B.A., Ortega, I., Hannlgan, J.W., Dammers, E., Shephard, M.W., Morris, E., Murph, K., Evans, M.J., Parrington, M., Whiyburn, S., Van Damme, M., Clarisse, L., Coheur, P., Clerbaux, C., Croft, B., Martin, R.V., Pierce, J.R., Fisher, J.A., 2019. Unprecedented ammonia concentrations detected in the high Arctic from the 2017 Canadian wildfire. J. Geophys. Res. Atmos. submitted.

Lynch, P., Reid, J.S., Westphal, D.L., Zhang, J., Hogan, T.F., Hyer, E.J., Curtis, C.A., Hegg, D.A., Shi, Y., Campbell, J.R., Rubin, J.I., Sessions, W.R., Turk, F.J., Walker, A.L., 2016. An 11-year global gridded aerosol optical thickness reanalysis (v1.0) for atmosphericand climate sciences. Geosci. Model Dev. 9, 1489–1522.

Markowicz KM, Pakszys P, Ritter C, Zielinski T, Udisti R, Cappelletti D, Mazzola M, Shiobara M, Xian P, Zawadzka O, Lisok J., 2016. Impact of North American intense fires on aerosol optical properties measured over the European Arctic in July 2015. Journal of Geophysical Research: Atmospheres.121(24):14-487.

Myhre, C.L., Toledano, C., Myhre, G., Stebel, K., Yttri, K.E., Aaltonen, V., Johnsrud, M., Frioud,

M., Cachorro, V., Frutos, A. de, 2007. Regional aerosol optical properties and radiative impact of the extreme smoke event in the European Arctic in spring 2006. Atmos. Chem. Phys. 7, 5899–5915.

O'Neill, N.T., Baibakov, K., Hesaraki, S., Ivanescu, L., Martin, R. V, Perro, C., Chaubey, J.P., Herber, A., Duck, T.J., 2016. Temporal and spectral cloud screening of polar winter aerosol optical depth (AOD): impact of homogeneous and inhomogeneous clouds and crystal layers on climatological-scale AODs. Atmos. Chem. Phys. 16, 12753–12765.

O'Neill, N.T., Eck, T.F., Smirnov, A., Holben, B.N., Thulasiraman, S., 2003. Spectral discrimination of coarse and fine mode optical depth. J. Geophys. Res. Atmos. 108.

O'Neill, N.T., Pancrati, O., Baibakov, K., Eloranta, E., Batchelor, R.L., Freemantle, J., Mcarthur, L.J.B., Strong, K., Lindenmaier, R., 2008. Occurrence of weak , sub-micron , tropospheric aerosol events at high Arctic latitudes 35. https://doi.org/10.1029/2008GL033733

O'Neill, N.T., Perro, C., Saha, A., Lesins, G., Duck, T.J., Eloranta, E.W., Nott, G.J., Hoffman, A., Karumudi, M.L., Ritter, C., 2012. Properties of Sarychev sulphate aerosols over the Arctic. J. Geophys. Res. Atmos. 117.

Peterson, D.A., Campbell, J., Hyer, E., Fromm, M., Kablick, G., Cossuth, J., DeLand, M., 2018. Wildfire-driven thunderstorms cause a volcano-like stratospheric injection of smoke. Clim Atmos Sci 1, 30.

Saha, A., O'Neill, N.T., Eloranta, E., Stone, R.S., Eck, T.F., Zidane, S., Daou, D., Lupu, A., Lesins, G., Shiobara, M., 2010. Pan-Arctic sunphotometry during the ARCTAS-A campaign of April 2008. Geophys. Res. Lett. 37.

Schoennagel, T., Balch, J.K., Brenkert-Smith, H., Dennison, P.E., Harvey, B.J., Krawchuk, M.A., Mietkiewicz, N., Morgan, P., Moritz, M.A., Rasker, R., 2017. Adapt to more wildfire in western North American forests as climate changes. Proc. Natl. Acad. Sci. 114, 4582–4590.

Sioris, C.E., Boone, C.D., Bernath, P.F., Zou, J., McElroy, C.T., McLinden, C.A., 2010. ACE observations of aerosol in the upper troposphere and lower stratosphere from the Kasatochi volcanic eruption. J. Geophys. Res 115, D00L14.

Soja, A.J., Tchebakova, N.M., French, N.H.F., Flannigan, M.D., Shugart, H.H., Stocks, B.J., Sukhinin, A.I., Parfenova, E.I., Chapin III, F.S., Stackhouse Jr, P.W., 2007. Climate-induced boreal forest change: predictions versus current observations. Glob. Planet. Change 56, 274–296.

Stohl, A., Andrews, E., Burkhart, J.F., Forster, C., Herber, A., Hoch, S.W., Kowal, D., Lunder, C., Mefford, T., Ogren, J.A., 2006. Pan-Arctic enhancements of light absorbing aerosol concentrations due to North American boreal forest fires during summer 2004. J. Geophys. Res. Atmos. 111.

Stone, R.S., Sharma, S., Herber, A., Eleftheriadis, K., Nelson, D.W., 2014. A characterization of Arctic aerosols on the basis of aerosol optical depth and black carbon measurements. Elem. Antropocene.

Tomasi, C., Kokhanovsky, A.A., Lupi, A., Ritter, C., Smirnov, A., O'Neill, N.T., Stone, R.S., Holben, B.N., Nyeki, S., Wehrli, C., 2015. Aerosol remote sensing in polar regions. Earth-Science Rev. 140, 108–157.

Tomasi, C., Lupi, A., Mazzola, M., Stone, R.S., Dutton, E.G., Herber, A., Radionov, V.F., Holben, B.N., Sorokin, M.G., Sakerin, S.M., 2012. An update on polar aerosol optical properties using POLAR-AOD and other measurements performed during the International Polar Year. Atmos. Environ. 52, 29–47.

Treffeisen RE, Thomason LW, Ström J, Herber AB, Burton SP, Yamanouchi T. Stratospheric Aerosol and Gas Experiment (SAGE) II and III aerosol extinction measurements in the Arctic middle and upper troposphere. Journal of Geophysical Research: Atmospheres. 2006 Sep 16;111(D17).

van der Werf, A., 2017. Growth analysis and photoassimilate partitioning, in: Photoassimilate Distribution Plants and Crops Source-Sink Relationships. Routledge, pp. 21–40.

van der Werf, G.R., Randerson, J.T., Giglio, L., Collatz, G.J., Kasibhatla, P.S., Arellano Jr, A.F., 2006. Interannual variability in global biomass burning emissions from 1997 to 2004. Atmos. Chem. Phys. 6, 3423–3441.

Viatte, C., Strong, K., Paton-Walsh, C., Mendonca, J.. O'Neill, N.T., Drummond, J.R., 2013. Measurements of CO, HCN, and C_2H_6 total columns in smoke plumes transported from the 2010 Russian boreal forest fires to the Canadian High Arctic. Atmos.-Ocean, 51 (5), 522–531.

Viatte, C., Strong, K., Hannigan, J., Nussbaumer, E., Emmons, L.K., Conway, S., Paton-Walsh, C., Hartley, J., Benmergui, J., Lin, J., 2015. Identifying fire plumes in the Arctic with tropospheric FTIR measurements and transport models. Atmos. Chem. Phys. 15, 2227–2246.

Viatte, C., Strong, K., Walker, K.A., Drummond, J.R., 2014. Five years of CO, HCN, C 2 H 6, C 2 H 2, CH 3 OH, HCOOH and H 2 CO total columns measured in the Canadian high Arctic. Atmos. Meas. Tech. 7, 1547–1570.

von Hardenberg, J. V, Vozella, L., Tomasi, C., Vitale, V., Lupi, A., Mazzola, M., Van Noije, T.P.C., Strunk, A., Provenzale, A., 2012. Aerosol optical depth over the Arctic: a comparison of ECHAM-HAM and TM5 with ground-based, satellite and reanalysis data. Atmos. Chem. Phys. 12.

Warneke, C., Froyd, K.D., Brioude, J., Bahreini, R., Brock, C.A., Cozic, J., De Gouw, J.A., Fahey, D.W., Ferrare, R., Holloway, J.S., 2010. An important contribution to springtime Arctic aerosol from biomass burning in Russia. Geophys. Res. Lett. 37.

3. Paper 2: Remote sensing of a high-Arctic, local dust event over Lake Hazen (Ellesmere Island, Nunavut, Canada)

Keyvan Ranjbar[a1], Norm T. O'Neill[a], Liviu Ivanescu[a], James King[b], Patrick L. Hayes[c]

[a] Centre d'Applications et de Recherches en Télédétection, Université de Sherbrooke, Sherbrooke, Canada

[b] Département de Géographie, Université de Montréal, Montréal, Québec, Canada

[c] Département de Chimie, Université de Montréal, Montréal, Québec, Canada

[1] Corresponding author Email address: keyvan.ranjbar@usherbrooke.ca

Keywords: Local Dust plume, Arctic-adapted RS techniques for dust detection, Dust optical properties, Drainage wind, High Arctic, Lake Hazen

Click here to download the supplementary Material: Supplementary info

Click here to download the supplementary Material: Supplementary Figures

Click here to download the supplementary Material: Movie S1

Click here to download the supplementary Material: Movie S2

Click here to download the supplementary Material: Data set S1

Click here to download the supplementary Material: Data set S2

Click here to download the supplementary Material: Data set S3

Abstract

A dust plume rising to a maximum altitude of about 1 km above the springtime high-Arctic terrain of Lake Hazen, Nunavut, Canada was detected using a diverse array of passive and active, satellite-based remote sensing techniques. We were able to broadly characterize the 532 nm optical depth and particle size of the upper plume (0.7 ± 0.1 and $18 – 25$ μm radius limits respectively). To our knowledge this is the first such remotely sensed, overland capture of what is an ubiquitous Aeolian process across the Arctic : drainage winds inducing dust plumes that are funneled along basin pathways to spread over the water and land surfaces at the outlets of those pathways. The identification and characterization of the Lake Hazen plume was challenging given that there is little development of passive and active remote sensing techniques over Arctic terrains. Our findings suggest that Arctic-adapted RS techniques that incorporate a priori information on dust optical properties can be exploited to identify and characterize locally generated plumes.

1 Introduction

Mineral aerosols constitute the largest uncertainty of global radiative forcing. This derives from uncertainties in their direct and indirect effects as well as in their frequency and magnitude (Boucher et al., 2013). Direct radiative impacts are responsible for up to 250 Wm^{-2} of surface insolation, while indirect feedbacks such as cloud production or suppression are equally important (Lohmann & Feichter, 2005; Tang et al., 2016). Additionally, mineral aerosols (MA) transport minor and trace elements important to ecological functions. MA also decrease air quality: this has health impacts on wildlife as well as in populated regions (Karanasiou et al., 2012).

Within arid regions, fugitive emissions of MA are the result of the availability of loose erodible material on the surface coupled with wind speeds that exceed the particle entrainment threshold. In most of these regions, erodible particles are always available or are renewed regularly by fluvial events. Wind events demonstrate synoptic, regional or jet-like characteristics with their relative importance being dependent on the geographical region. However, there is a growing recognition of the importance of jet-like flows (e.g., nocturnal low-level jet) for generating emissions (Washington and Todd, 2005) inasmuch as their high frequency relative to synoptic scale generated winds, are not transport capacity dependent (Allen et al., 2013). Drainage flows (which include katabatic flows) are a sub-class of jet-like flows: they are generated in mountainous regions and have diurnal frequencies with extremely high near-surface winds independent of synoptic

systems. Winds generated by these flows drive emissions of high latitude MA (HLMA). They are influenced by mountain topography and large temperature contrasts: more regional or synoptic components cannot develop enough energy.

HLMA have recently been identified as a potentially strong influence on climate (Bullard et al., 2016). These influences exceed (per unit mass), those of MA that are produced, transported, and deposited at lower latitudes. This is ascribed to the high likelihood of HLMA (depositing on snow, ice and frozen bare ground) increasing snow or ice ablation rates as well as the increased effects of nutrient deposition (e.g., Fe, P) within a highly disconnected and nutrient limited landscape and the attendant increase in terrestrial and aquatic productivity (Schroth et al., 2017). Furthermore, with the influence of anthropogenic climate change being enhanced in polar regions (Lehnherr et al., 2018), it is hypothesized that the number and frequency of emissions of Arctic-based MA could increase as snow and ice coverage decrease, summer seasons elongate, and precipitation patterns change (Bullard et al., 2016).

Despite the potential for HLMA playing an important global-climate role, their geographical identification, frequency, and intensity, outside of several well-monitored research areas, are not well known. Those that have been identified and researched include several sources in Iceland (Baddock et al., 2017; Prospero et al., 2012) and Greenland (Bullard and Mockford, 2018). Distinct sources within North America include the Copper River, Alaska (Crusius et al., 2011), Kluane Lake, Yukon (Bachelder et al., 2020), and southern Baffin Island, Nunavut (Neuman, 1990). With the identification of other HLMA sources (from World Meteorological Organization weather codes for blowing dust as per Engelstaedter et al., 2003) , it is suggested that between 3% and 5% of the global dust budget (Bullard et al., 2016) or around 5 – 10 Mt originates from high latitudes (Zwaaftink et al., 2016). With a sparse monitoring network and known seasonality of small source regions (hindering the ability to identify and quantify contributions), this likely underestimates the ratio of HLMA to global mineral aerosol emissions.

Remote sensing images acquired using passive sensors aboard various satellite platforms enhance our ability to identify and characterize aerosol-plume events using multi-spectral (e.g., MODIS, VIIRS, Aerosol Index images produced by OMI) and multi-angle (e.g., MISR and PARASOL) techniques while active sensors (notably the CALIOP lidar) provide vertical profile

and some speciation capabilities to support the identification and characterization of aerosol events. There are numerous examples in the literature on the active and passive remote sensing of wind-eroded desert dust plumes at southern latitudes (see, for example, Xie et al., 2017 and Hsu et al., 2013 for remote sensing investigations over the Chinese and Saharan desert and Huang et al., 2008 and Peyridieu et al., 2013 for investigations of dust plumes over the Pacific and Atlantic Ocean). To date, the capture of HLMA events using RS techniques has, however, been limited to plumes over water (see for example, Crusius et al. (2011) for an event captured using MODIS visible imagery over the Gulf of Alaska). Vincent (2018) reported on the detection of summertime dust plumes ascribed to Asian and local dust using MODIS Brightness Temperature Differences (BTDs) over the Amundsen Gulf in the Western Canadian Arctic (with channels identical to the those employed for MODIS BTDs we present below): however, given the ubiquitous presence of Boreal forest fires in northern Canada and the generally pervasive optical dominance of smoke during the summer period, we are wary of the claim that the thick plumes seen in the MODIS imagery shown in that paper are dust (comment in preparation). There is substantial remote sensing literature on the inference of mid-latitude dust transport and subsequent dust deposition effects derived from changes in the surface reflectance of snow or ice in mountainous regions (see, for example Painter et al., 2012 and Seidel et al., 2016).

The products of aerosol remote sensing sensors are often not attuned to the unusual conditions such as those found in the Arctic. In this study we demonstrate how the multi-dimensional information content of four sensors (MODIS, MISR, CALIOP and CloudSat) was exploited and readapted to identify a singular springtime (May) plume event over Lake Hazen, Nunavut in the Canadian high Arctic.

2 Relevant site information

2.1 Lake Hazen

Lake Hazen is located on Ellesmere Island in the territory of Nunavut, Canada. It extends from about 81.7°N 73.0°W to 81.9°N 68.9°W and is the Arctic's largest lake, by volume (51.4 km^3). Figure 1 delineates the Lake Hazen watershed, the different glaciers in that watershed as well as the glacial rivers associated with the sub-watersheds of each glacier. Lake Hazen camp (also known as Hazen base camp), is indicated on the north shore of the lake.

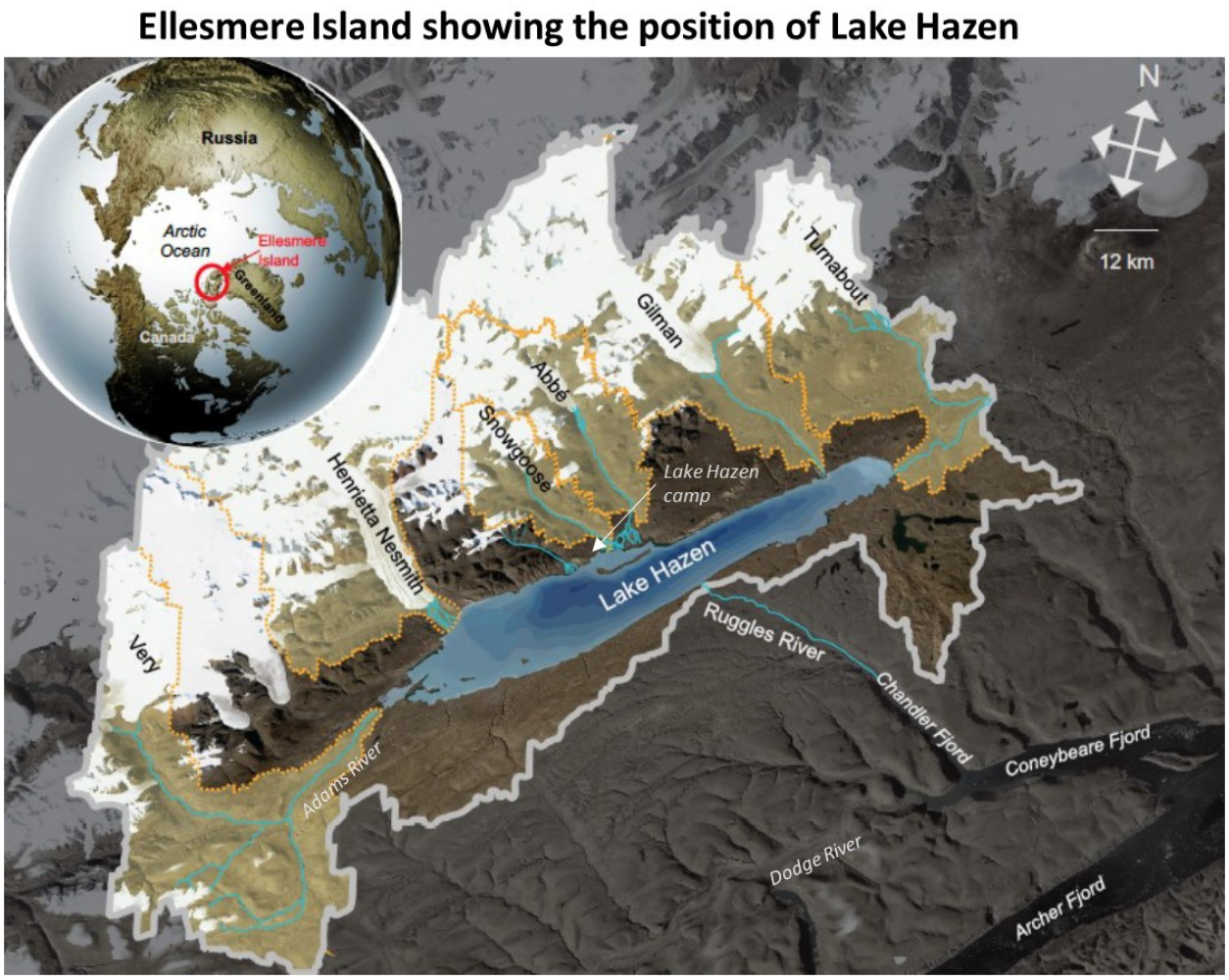

Figure 2. Map of the Lake Hazen watershed (grey outline) on northern Ellesmere Island (see inset map). Major hydrologic features as well as associated glaciers are identified (sub-watersheds are delineated in orange). Important Lake Hazen glacial rivers are shown in cyan (as well as Dodge River feeding into Coneybeare Fjord). Adapted from St Pierre (2018).

2.2 Brief climatology of Lake Hazen

Hudson et al. (2001) present a climatological overview of Nunavut and Arctic weather with a brief section on Lake Hazen. The Lake Hazen watershed is classified as a semi-polar desert and is known as a high Arctic "thermal oasis" (St Pierre, 2018). Jackson (1960) underscored the generally unique calmness of Lake Hazen in contrast to a coastal site such as Alert (~120 km to the northeast). There exists no recent Lake Hazen climatic data archives that include the dust event that we describe below. We did, however, find a five-year climatic data set for Lake Hazen camp

(2008 to 2012) that we have included in the Data Set S1. The temperature statistics for the month of May (computed from the ensemble of daily averages during this 5-year period), show an average temperature of -3.8 ± 3.0 °C with a 0 °C crossing typically occurring in early June.

There are few temperature radiosondes over Lake Hazen reported in the published and unpublished literature. Figures S1 to S5 show four vertical profiles acquired along a rare 10 April 2015 flight from Alert to Eureka (about 150 km northeast and 330 km southwest of Lake Hazen camp respectively): an ascent from Alert, a descent from Lake Hazen, an ascent from Tanquary Fjord and a relatively tight spiral descent to Eureka. One can see boundary layer temperature inversions for the Alert and Eureka flight segments while the Lake Hazen and Tanquary Fjord segments show no inversions. The less sheltered sites of Alert and Eureka are apparently subject to the more regional and strong Arctic inversions characteristic of the polar winter and spring (Bradley et al., 1993) while the more sheltered Lake Hazen and Tanquary Fjord profiles are not incoherent with Jackson's (1965) inference of a shallow summertime inversion layer over Lake Hazen (and by extension a progressive transformation from a strong polar winter inversion to less extreme inversion conditions during the late spring and summer).

2.3 Drainage winds over Lake Hazen

Our analysis of the 2008 to 2012 wind speed data showed a high degree of variability and a year to year increasing trend that was difficult to justify given the available supporting information. We chose instead to use an older 12-year (1988 to 1999) Lake Hazen climate data set that showed a more consistent year to year variability (c.f. Data Set S2). The ensemble of daily wind velocity results for the 12 year Lake Hazen archive (see Figure S6) indicates the predominance of calm winds for the majority of time with distinct high wind events likely associated with topographically induced drainage (Jackson, 1960). Previous research has determined daily windspeed thresholds for emissions to range from 4 to 7 $m\text{-}s^{-1}$ depending on the soil conditions (Stout, 2001; Whicker et al., 2002). The ensemble wind velocity results for the 12-year Lake Hazen archive shows that during the month of May, daily windspeeds greater than 4 and 7 $m\text{-}s^{-1}$ occurred 6.5 and 4.0% of the time, respectively.

3 RS tools

3.1 MISR

MISR, on board the Terra satellite, provides near simultaneous observations at nine viewing angles in three VIS and one NIR band (see Figure S7 and S8, respectively, for details concerning those viewing angles and sample images on the day of the Lake Hazen dust event). MISR has a much narrower swath width than the MODIS imager (380 km versus 2330 km). Stereoscopic techniques applied to co-registered layers of the different angular views enables construction of 3-D models that yield images of aerosol or cloud plume height as well as the horizontal velocities of matching plume pixels. At the same time, the contextual capability of visually confirming the movement of unique portions of a plume is a means of adding confidence to the automated matching exercise of extracting plume altitude and speed.

3.2 MODIS

The MODIS imagers aboard the Terra and Aqua satellites acquire UV to thermal-IR imagery in 36 bands across a 2330 km swath at a spatial resolution varying from 250 to 1000 m. The fact that MISR and MODIS-Terra share the same Terra platform provides simultaneous observations which synergize their remotely sensed information content. The broad spectral range of MODIS imagery enables the extraction of aerosol / cloud information that complements the MISR retrieval products. However, snow / ice surfaces and low solar zenith angles complicate aerosol, solar-reflective retrievals over the Arctic (see, for example, Mei et al., 2013).

A dust RS approach with a longer heritage than solar reflective techniques is the BTD technique involving pairs of TIR (thermal IR) bands (see, for example, Miller et al. (2017) for an overview of different BTD techniques). A BT, sensitive to higher altitude plume absorption and / or scattering interactions in a given TIR band is subtracted from a BT reference that is highly transmitting and more sensitive to the surface BT. Ackerman (1997) presented two robust BTD indicators that could be employed for dust discrimination in the presence of competing signals such as clouds, sea surface and different types of desert surfaces. From dust-free (background) parts of a scene to regions of thick dust, the two BTDs employed ($BT_{8.5} - BT_{11}$ and $BT_{11} - BT_{12}$) showed a tendency, respectively, for large negative values tending toward small positive values and positive values leading towards small negative values (where the subscripts “8.5”, “11” and

"12" refer to approximate band centers in μm and, in the case of MODIS to bands 29, 31 and 32 respectively). These BTD techniques were, however, generally limited to warm desert scenes: their extension to the detection of a dust plume over a heterogeneous high-Arctic surface is discussed below.

3.3 CALIOP and CloudSat

The CALIOP aerosol/cloud lidar aboard the CALIPSO satellite produces two dimensional "curtains" of 532 nm backscatter profiles along a polar-orbit track. The cloud profiling radar aboard the CloudSat satellite produces analogous backscatter curtains in the same (A-train) polar orbit (MODIS-Aqua, CALIOP and CloudSat were all members of the A-train at the time of this event; CALIOP and CloudSat have recently been moved to a lower orbit). The 3D cross section perspective from the intersection of CloudSat/CALIOP profiles and MODIS-Aqua imagery as well as MISR multi-angle imagery and MODIS-Terra imagery provides a valuable spatial contextualization tool for identifying and understanding particulate backscatter events. An overview description of CALIOP and its processing algorithms can be found in Winker et al. (2009). A similar document for CloudSat can be found in Stephens et al. (2008).

3.4 General comments

The polar orbits of the CALIOP, CloudSat, MISR and MODIS platforms enable a much larger satellite product density in time and space at high latitudes as compared to more southern sites. This largely ensures the identification of any optically significant aerosol event on any given day (cloud cover being virtually the only constraint in at least visually identifying such an event).

4 Local Dust event description:

Movie S1 shows a video of the dust storm made by a ground party at Lake Hazen camp on the morning of 20 May while Figure S9 shows photos taken before and after the dust event (16 May and 20 May respectively). The latter photo was taken at 16:02 local time (12:02 UT): the general calm nature of the scene relative to the time of acquisition of our key MODIS-Terra image (discussed immediately below) indicates that the dust storm ended rather abruptly.

4.1 Identification of the dust plume

Figure 2a shows a true-color georeferenced, RGB MODIS-Terra image acquired on 19 May 2014 at 19:50 UT (15:50 EDT) clipped to the area of Figure 1. One can distinguish glaciers and snow / ice covered terrain, what appears to be a mostly ice / snow covered Lake Hazen, dust on the ground about and on the lake as well as the Adams River basin and, as we argue below, a distinct dust plume. One can also make analogous surface-dust affirmations in the region of the Dodge River and other tributaries. The blue broken-line square at the bottom of Figure 2a shows a zoom of a conical structure that we believe to be a dust plume. In this section we try to validate this visual affirmation.

Figure S10 incorporates an animation of the 9 MISR true-color images acquired by the 9 forward to aft cameras. It shows the conical structure of Figure 2a apparently emanating from the Adams River basin and moving in a northeast direction. We would expect this movement to be observable given the eye's capability of following the coherent motion of complex objects: the apparent velocity of the plume (core velocities of $<\sim 10$ m-s^{-1} as discussed below) and the 7 minutes needed to acquire the 9 MISR Lake Hazen images (Nelson et al., 2013) means that the plume will have moved $<\sim 4.2$ km or $<\sim 15$ MISR pixels during that 7 minute period.

The implementation of the desert dust BTD methodology discussed above to the high Arctic case of the Lake Hazen plume also needs justification. Aside from the large changes in temperature magnitudes from a desert to a high Arctic environment we have argued above for a Lake Hazen thermal environment that does not include a temperature inversion (or at least not a strong temperature inversion). Figure S11 also suggests that such a thermal lapse rate existed on 19 May 2014: the superposition of the MODIS BT_{11} (high transmission, reference) image on the MISR-generated elevation model generally supports the absence of an inversion layer. Ackerman's BTD development included the reference to the background desert aerosol (fine mode aerosols with a radius peak ~ 0.1 μm and very small single scattering albedo values (strong absorption) around 8.5 μm). Such a background aerosol is quite similar to ubiquitous Arctic haze aerosols in general: Ritter et al. (2005), for example, measured substantial TIR optical depth values (at the high Arctic site of Ny Alesund) which they attributed to the strongly absorbing nature of sulfate aerosols in the TIR.

Figure 2b shows the BTD (BT_{11}– BT_{12}) image corresponding to the MODIS RGB image of Figure 2a. A clear (negative) minimum in the neighborhood of the thickest portion of the RGB plume can be observed. To better understand the interdynamics between the BT images relative to the RGB image the reader can consult Figures S12 and S13. A similar degree of (positive) plume discrimination was observed for the $BT_{8.5}$– BT_{11} image (the same sequence of alternating images is shown in Figures S14 and S15).

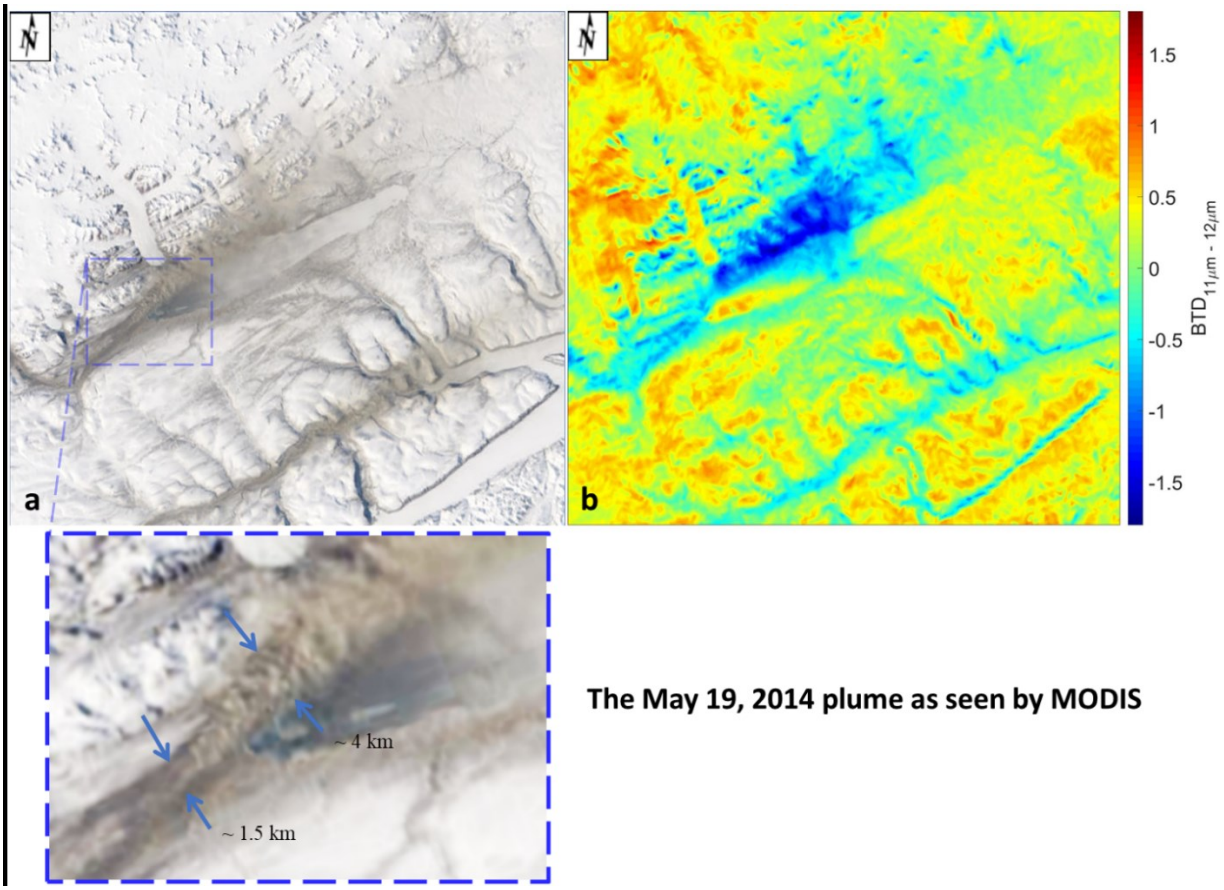

Figure 2. MODIS-Terra 19 May 2014, 19:50 UTC (a) RGB image. (b) BTD = BT11 – BT12. Details on the bands employed are given in the Figure S12 caption.

4.2 Plume height and speed

Figure 3 shows the wind-corrected plume height (km ASL) superimposed on the MISR RGB, nadir image. The largest and most dense collection of plume height retrievals correspond well with the thick Adams River plume that was visually and thermally identified in the previous section. Figure 4a shows the corresponding MISR-derived, zero-wind heights, wind-corrected heights, and

terrain height for pixels along the 12:06 UT CALIOP orbit line (the purple broken line of Figure 3). Figure 4b shows the CALIOP 532 nm total attenuated backscatter profile. The high values of total attenuated backscatter coefficient outlined by the two yellow rectangles are in about the same position and height along the CALIOP orbit line as the two height peaks of the MISR profile. We presume that the fact that CALIOP does not show an obvious return over Lake Hazen (where MISR appears to detect a 3rd lower plume) is due to the nearly 8 hours of difference in the acquisition of the MISR image and the CALIOP profile).

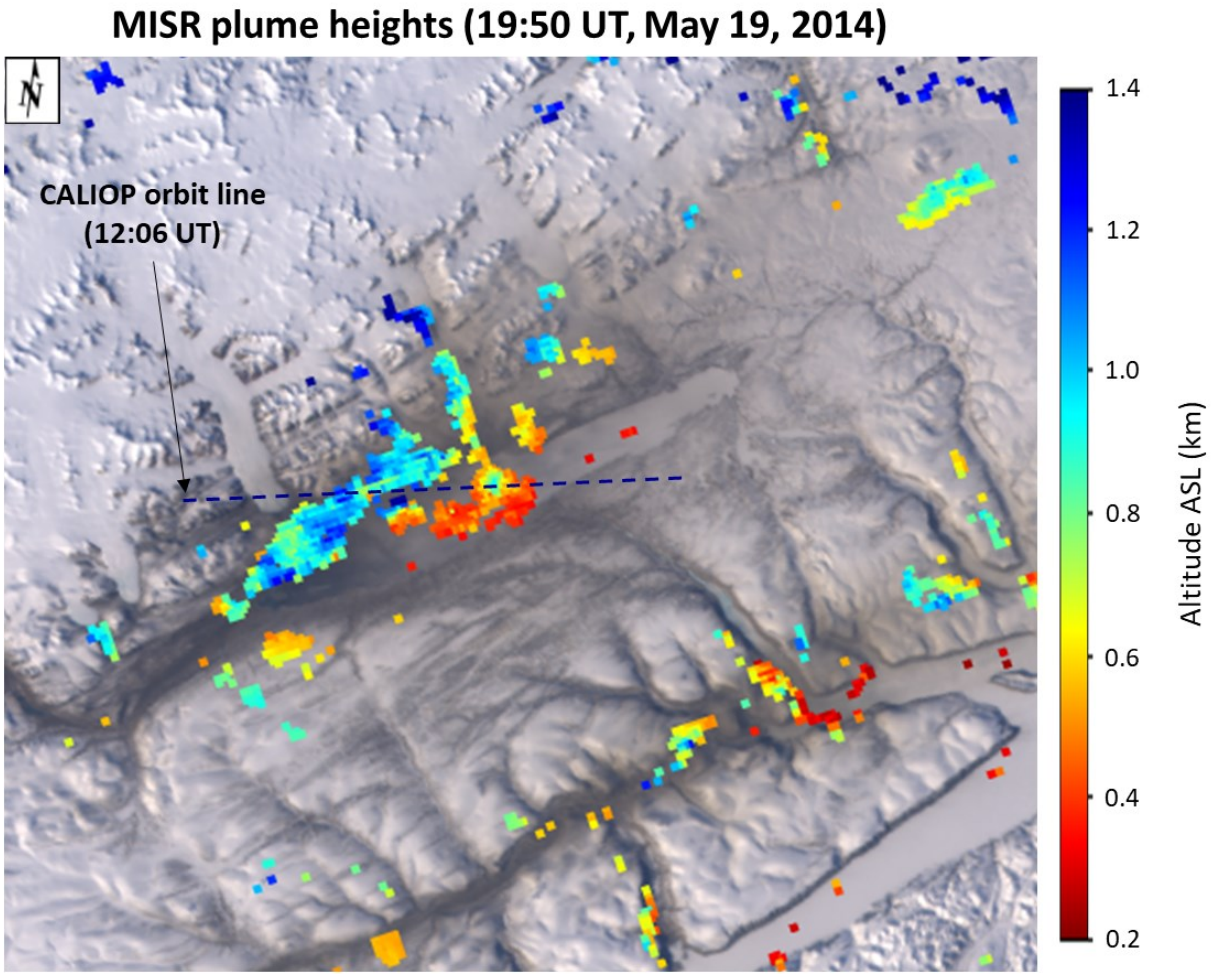

Figure 3. 19 May 2014, MISR wind-corrected heights superimposed on the MISR RGB, nadir image (algorithmic details are given in the Figure S14 caption). The heights are represented by a red to blue color scale (using a color-activation threshold of 200 m). The purple dashed line shows the orbit line of the Figure 4b (CALIOP) altitude profile.

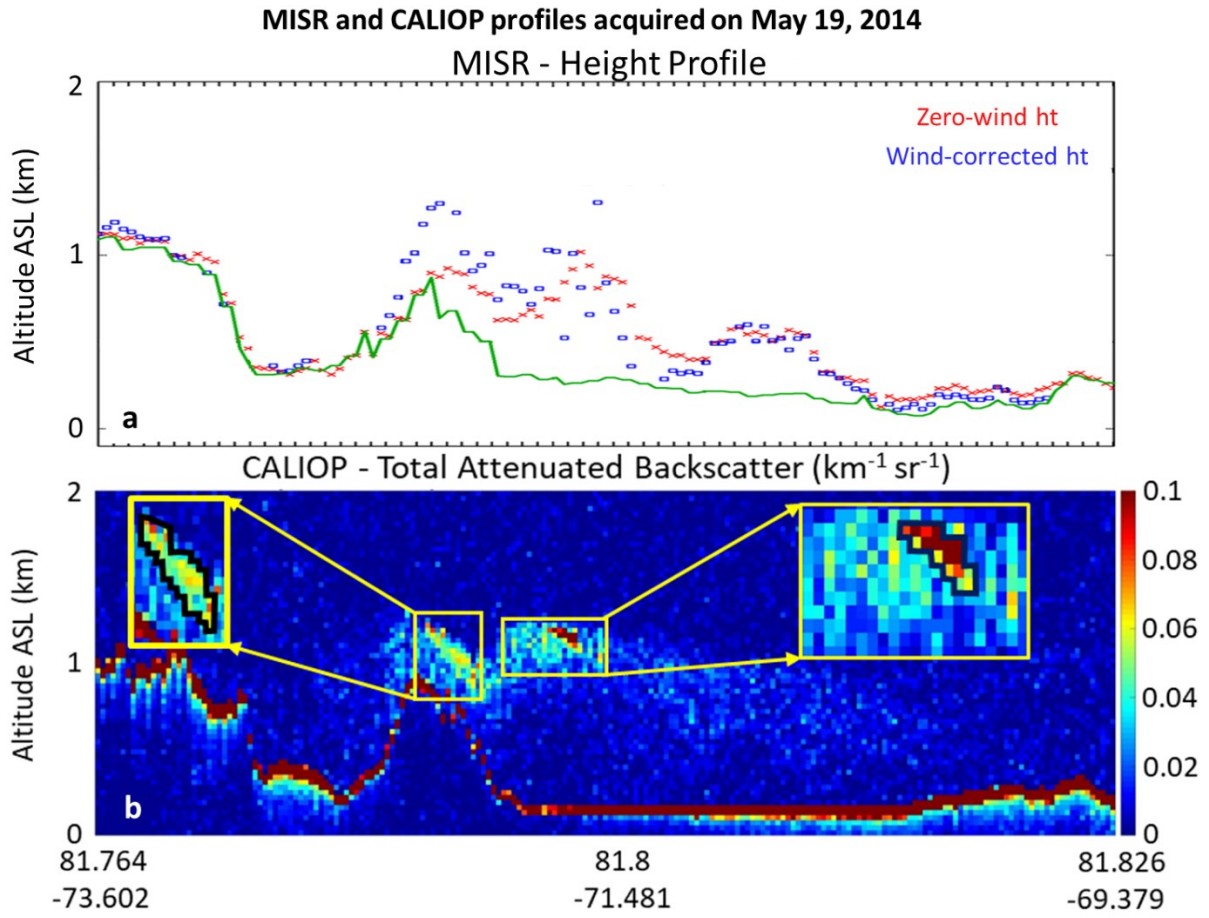

Figure 3. (a) MISR plume height and (b) CALIOP total attenuated backscatter coefficient. The MISR profile corresponds to the height information of Figure 3 where the heights are constrained to pixels along the purple-dashed (CALIOP) orbit line. The CALIOP profile was acquired at 12:06 UT (about 7 hours and 40 minutes before the MISR overpass). Details on the CALIOP profile can be found in the Figure S25 caption.

An image of MISR-derived total wind speed is shown in Figure S17. While that image does show maximum values for the Adams River plume, they are not inordinately large (<~ 10 m-s^{-1}). However, as indicated above, the speed of drainage flows are typically known to decrease significantly with increasing altitude (see Renfrew & Anderson, 2006 for example). NOAA reanalysis data (2.5º grid cells) indicated a general increase in regional wind speeds in the northern half of Ellesmere Island (Tanquary Fjord, Lake Hazen, and Alert) rising from about 4 m-s^{-1} on 17 May to around 8 m-s^{-1} on 19 May (c.f. Data Set S3). This increase suggests a link between the reanalyzed wind fields and the low level MISR-derived drainage flow wind speeds.

4.3 Characterization of dust properties

The MODIS aerosol optical depth process failed to detect aerosols (let alone dust aerosols). The vast majority of plume pixels were classified as clouds by the CALIOP classification process (Figure S19). The combined CALIOP/CloudSat ice cloud classification process does not include an aerosol classification product (c.f. Figure S20). The DARDAR (CALIOP, CloudSat, CALIPSO IR imager) classification product (DARDAR-MASK) includes aerosol classification but no pixels were classified as aerosols (Figure S21).

In order to at least obtain order of magnitude estimates of optical depth and effective particle radius (r_{eff}) of the upper plume (defined by the highest S/N area of the plume in Figure 4b) we employed the DARDAR retrievals as a baseline from which uncertainties could be calculated assuming that dust (or ice-coated dust) particles of the plume were mis-classified as ice particles: i.e. the order of magnitude differences in the basic optical properties of ice-cloud particles relative to those of dust particles were converted to order of magnitude errors in the retrieval products of optical depth and r_{eff} (see details in Text S1). This yielded a 532 nm optical depth estimate of ~ 0.7 ± 0.1 and broad r_{eff} limits of ~ 18 – 25 μm for upper plume particles (where the r_{eff} upper bound error was reset, relative to the nominal retrieval uncertainties, given published field evidence for the maximum particle size that could be transported across the estimated distance from the source of our upper plume (~ 10 km)).

5 Conclusions

A high Arctic dust plume over the complex ice, snow and dust imbedded terrain of the Lake Hazen, Nunavut watershed was detected using a diverse array of passive and active, satellite-based remote sensing techniques. In addition we were able to broadly characterize the 532 nm optical depth and particle size of the upper plume (0.7 ± 0.1 and 18 – 25 μm radius limits respectively). These "giant" dust particles (see for example, Weinzierl et al., 2009) are limited to transport distances <~ 10 km.

To our knowledge this is the first such remotely sensed, overland capture of what is a ubiquitous Aeolian process across the Arctic : drainage winds inducing dust plumes that are funnelled along basin pathways to spread over the water and land surfaces at the outlets of those pathways. The identification and characterization of the Lake Hazen plume was challenging given that there is

little development of passive and active remote sensing techniques over Arctic terrains and that these techniques, as well as active techniques (CALIOP and CloudSat) failed to identify the dust nature of the plume.

The apparent effects of dust deposition and/or dust erosion on the dust plume pathway along and beyond the Adams River basin outlet can, to a degree, be discerned over 20 years of MODIS imagery in the region of the Lake Hazen watershed (Movie S2). Woo et al. (1991) observed snow-melt zones on the Fosheim Pennisula (the location of Eureka) that corresponded to "dark spots" on a map derived from NOAA imagery (AVHRR 1 km resolution imagery acquired on 17 May 1990). They noted that the first area to experience significant snow melt in their map zone was dust covered. We found what appeared to be snow-free and/or dust covered watershed patterns in MODIS imagery to be readily observable as dark / brownish features across Ellesmere Island on the day of our dust event (see the Figure S24 to S28 illustrations). In particular, that imagery when clipped to the dimensions of Woo et al's AVHRR-derived map shows rather remarkable spatial correlation with their "dark spots" taken 24 years earlier (see Figure S29).

A hypothesis that the darkening/browning of snow or ice covered Arctic surfaces is largely the result of wind blown dust deposition suggests a means of searching for potential dust plumes by employing reflectance changes in the basin pathways as flags for their presence. One could then focus passive and active remote sensing techniques (multi-angle imagery, satellite-based lidar and radar profiles, BTD imagery, etc) near the outlets or along the basin pathways to search for plumes. This systematic identification and subsequent characterization of dust plumes would be valuable in better understanding the driving mechanisms that generate the apparent dust covered snow / ice surfaces along watershed pathways.

The comprehensive review of Bullard et al. (2016) on the importance of high latitude dust to the earth system underscored the limitations of remotely sensed information on locally generated high latitude dust. Our findings suggest that remote sensing retrieval techniques, adapted to the special conditions of the Arctic landscape and incorporating a priori information on dust optical properties can be better exploited to first flag and then investigate locally generated dust plumes over the large expanses of Arctic area where there can be no practical aspirations of deploying dedicated sites or measurement campaigns. This approach must necessarily take full advantage of

the newest and upcoming generation of aerosol- and cloud-dedicated, multi-dimensional sensors (TROPOMI and VIIRS, the EarthCare ATLID lidar and CPR radar, the A-CCP missions, etc.).

6 Acknowledgements

We gratefully acknowledge funding from the PAHA project (NSERC-CCAR program; RGPCC-433842-2012), the SACIA project (CSA-ESSDA program; 16UASACIA), the CMN (NCE program; RES0044975) and the NSERC DG grants of Hayes, King and O'Neill (RGPIN-2017-05531, RGPIN-2016-05417 and RGPIN-05002-2014). We also gratefully acknowledge usage of data from the following sites; https://eosweb.larc.nasa.gov/project/calipso/calipsotable (CALIOP data), http://www.cloudsat.cira.colostate.edu/order-data (CloudSat data), http://www.icare.univ-lille1.fr/projects/dardar (DARDAR data), https://ladsweb.modaps.eosdis.nasa.gov/search/ (MODIS data), https://l0dup05.larc.nasa.gov/MISR/cgi-bin/MISR/main.cgi (MISR data), https://psl.noaa.gov/data/composites/hour/ (reanalysis data) and https://climate.weather.gc.ca/historical_data/search_historic_data_e.html (weather data).

7 References

Ackerman, S.A., 1997. Remote sensing aerosols using satellite infrared observations. J. Geophys. Res. Atmos. 102, 17069–17079.

Allen, C.J.T., Washington, R., Engelstaedter, S., 2013. Dust emission and transport mechanisms in the central Sahara: Fennec ground-based observations from Bordj Badji Mokhtar, June 2011. J. Geophys. Res. Atmos. 118, 6212–6232.

Bachelder, J., Cadieux, M., Liu-Kang, C., Lambert, P., Filoche, A., Galhardi, J.A., Hadioui, M., Chaput, A., Bastien-Thibault, M.-P., Wilkinson, K.J., King, J., Hayes, P.L., 2020. Chemical and microphysical properties of wind-blown dust near an actively retreating glacier in Yukon, Canada. Aerosol Sci. Technol. 54, 2–20.

Baddock, M.C., Mockford, T., Bullard, J.E., Thorsteinsson, T., 2017. Pathways of high-latitude dust in the North Atlantic. Earth Planet. Sci. Lett. 459, 170–182.

Boucher, O., Randall, D., Artaxo, P., Bretherton, C., Feingold, G., Forster, P., Kerminen, V.-M., Kondo, Y., Liao, H., Lohmann, U., 2013. Clouds and aerosols, in: Climate Change 2013: The Physical Science Basis. Contribution of Working Group I to the Fifth Assessment Report of the Intergovernmental Panel on Climate Change. Cambridge University Press, pp. 571–657.

Bradley, R.S., Keimig, F.T., Diaz, H.F., 1993. Recent changes in the North American Arctic boundary layer in winter. J. Geophys. Res. Atmos. 98, 8851–8858.

Bullard, J.E., 2013. Contemporary glacigenic inputs to the dust cycle. Earth Surf. Process. Landforms 38, 71–89.

Bullard, J.E., Baddock, M., Bradwell, T., Crusius, J., Darlington, E., Gaiero, D., Gasso, S., Gisladottir, G., Hodgkins, R., McCulloch, R., 2016. High-latitude dust in the Earth system. Rev. Geophys. 54, 447–485.

Bullard, J.E., Mockford, T., 2018. Seasonal and decadal variability of dust observations in the Kangerlussuaq area, west Greenland. Arctic, Antarct. Alp. Res. 50, S100011.

Crusius, J., Schroth, A.W., Gasso, S., Moy, C.M., Levy, R.C., Gatica, M., 2011. Glacial flour dust storms in the Gulf of Alaska: Hydrologic and meteorological controls and their importance as a source of bioavailable iron. Geophys. Res. Lett. 38.

Delanoë, J., Hogan, R., 2010. DARDAR-CLOUD.

Deng, M., Mace, G.G., Wang, Z., Okamoto, H., 2010. Tropical Composition, Cloud and Climate Coupling Experiment validation for cirrus cloud profiling retrieval using CloudSat radar and CALIPSO lidar. J. Geophys. Res. Atmos. 115.

Donovan, D.P., Van Lammeren, A., 2001. Cloud effective particle size and water content profile retrievals using combined lidar and radar observations: 1. Theory and examples. J. Geophys. Res. Atmos. 106, 27425–27448.

Engelstaedter, S., Kohfeld, K.E., Tegen, I., Harrison, S.P., 2003. Controls of dust emissions by vegetation and topographic depressions: An evaluation using dust storm frequency data. Geophys. Res. Lett. 30.

Esselborn, M., Wirth, M., Fix, A., Weinzierl, B., Rasp, K., Tesche, M., Petzold, A., 2009. Spatial distribution and optical properties of Saharan dust observed by airborne high spectral resolution lidar during SAMUM 2006. Tellus B Chem. Phys. Meteorol. 61, 131–143.

Grenier, P., Blanchet, J., Muñoz-Alpizar, R., 2009. Study of polar thin ice clouds and aerosols seen by CloudSat and CALIPSO during midwinter 2007. J. Geophys. Res. Atmos. 114.

Gustafson, B.Å.S., Kolokolova, L., Xu, Y., Greenberg, J.M., Stognienko, R., 2001. Interactions with electromagnetic radiation: Theory and laboratory simulations, in: Interplanetary Dust. Springer, pp. 509–567.

Hsu, N.C., Jeong, M., Bettenhausen, C., Sayer, A.M., Hansell, R., Seftor, C.S., Huang, J., Tsay, S., 2013. Enhanced Deep Blue aerosol retrieval algorithm: The second generation. J. Geophys. Res. Atmos. 118, 9296–9315.

Huang, J., Minnis, P., Chen, B., Huang, Z., Liu, Z., Zhao, Q., Yi, Y., Ayers, J.K., 2008. Long-range transport and vertical structure of Asian dust from CALIPSO and surface measurements during PACDEX. J. Geophys. Res. Atmos. 113.

Hudson, E., Aihoshi, D., Gaines, T., Simard, G., Mullock, J., 2001. The weather of Nunavut and

the Arctic, Graphical area forecast 36 and 37. Nav Canada.

Jackson, C.I., 1965. The Vertical Profile of Wind at Lake Hazen, NWT. Arctic 18, 21–35.

Jackson, C.I., 1960. The Meteorology of Lake Hazen, Ellesmere Island, NWT. McGill University, Montreal.

Karanasiou, A., Moreno, N., Moreno, T., Viana, M., De Leeuw, F., Querol, X., 2012. Health effects from Sahara dust episodes in Europe: literature review and research gaps. Environ. Int. 47, 107–114.

Kim, M.-H., Omar, A.H., Tackett, J.L., Vaughan, M.A., Winker, D.M., Trepte, C.R., Hu, Y., Liu, Z., Poole, L.R., Pitts, M.C., 2018. The CALIPSO version 4 automated aerosol classification and lidar ratio selection algorithm. Atmos. Meas. Tech. 11.

Lehnherr, I., Louis, V.L.S., Sharp, M., Gardner, A.S., Smol, J.P., Schiff, S.L., Muir, D.C.G., Mortimer, C.A., Michelutti, N., Tarnocai, C., 2018. The world's largest High Arctic lake responds rapidly to climate warming. Nat. Commun. 9, 1–9.

Lewicki, S.A., Zong, J., 1999. MISR Level 1 ancillary geographic product algorithm theoretical basis. JPL Tech. Doc. D-13400, Rev. A.

Lohmann, U., Feichter, J., 2005. Global indirect aerosol effects: a review. Atmos. Chem. Phys. 5, 715–737.

Mace, G., Deng, M., 2019. Level 2 CloudSat-CALIPSO Combined Ice Cloud Property Retrieval Product Process Description and Interface Control Document.

Madonna, F., Amodeo, A., D'Amico, G., Pappalardo, G., 2013. A study on the use of radar and lidar for characterizing ultragiant aerosol. J. Geophys. Res. Atmos. 118, 10–56.

Mei, L., Xue, Y., de Leeuw, G., von Hoyningen-Huene, W., Kokhanovsky, A.A., Istomina, L., Guang, J., Burrows, J.P., 2013. Aerosol optical depth retrieval in the Arctic region using MODIS data over snow. Remote Sens. Environ. 128, 234–245.

Miller, S.D., Bankert, R.L., Solbrig, J.E., Forsythe, J.M., Noh, Y., Grasso, L.D., 2017. A Dynamic Enhancement With Background Reduction Algorithm: Overview and Application to Satellite-Based Dust Storm Detection. J. Geophys. Res. Atmos. 122, 12–938.

Nelson, D.L., Garay, M.J., Kahn, R.A., Dunst, B.A., 2013. Stereoscopic height and wind retrievals for aerosol plumes with the MISR INteractive eXplorer (MINX). Remote Sens. 5, 4593–4628.

Neuman, C.M., 1990. Observations of winter aeolian transport and niveo-aeolian deposition at Crater Lake, Pangnirtung Pass, NWT, Canada. Permafr. Periglac. Process. 1, 235–247.

Omar, A., Liu, Z., Vaughan, M., Thornhill, K., Kittaka, C., Ismail, S., Hu, Y., Chen, G., Powell, K., Winker, D., 2010. Extinction-to-backscatter ratios of Saharan dust layers derived from in situ measurements and CALIPSO overflights during NAMMA. J. Geophys. Res. Atmos. 115.

Painter, T.H., Bryant, A.C., Skiles, S.M., 2012. Radiative forcing by light absorbing impurities in snow from MODIS surface reflectance data. Geophys. Res. Lett. 39.

Peyridieu, S., Chédin, A., Capelle, V., Tsamalis, C., Pierangelo, C., Armante, R., Crevoisier, C., Crépeau, L., Siméon, M., Ducos, F., 2013. Characterisation of dust aerosols in the infrared from IASI and comparison with PARASOL, MODIS, MISR, CALIOP, and AERONET observations.

Prospero, J.M., Bullard, J.E., Hodgkins, R., 2012. High-latitude dust over the North Atlantic: inputs from Icelandic proglacial dust storms. Science (80-.). 335, 1078–1082.

Renfrew, I.A., Anderson, P.S., 2006. Profiles of katabatic flow in summer and winter over Coats Land, Antarctica. Q. J. R. Meteorol. Soc. A J. Atmos. Sci. Appl. Meteorol. Phys. Oceanogr. 132, 779–802.

Ritter, C., Notholt, J., Fischer, J., Rathke, C., 2005. Direct thermal radiative forcing of tropospheric aerosol in the Arctic measured by ground based infrared spectrometry. Geophys. Res. Lett. 32.

Schroth, A.W., Crusius, J., Gassó, S., Moy, C.M., Buck, N.J., Resing, J.A., Campbell, R.W., 2017. Atmospheric deposition of glacial iron in the Gulf of Alaska impacted by the position of the Aleutian Low. Geophys. Res. Lett. 44, 5053–5061.

Seidel, F.C., Rittger, K., Skiles, S.M., Molotch, N.P., Painter, T.H., 2016. Case study of spatial and temporal variability of snow cover, grain size, albedo and radiative forcing in the Sierra Nevada and Rocky Mountain snowpack derived from imaging spectroscopy. Cryosph. 10.

St Pierre, K., 2018. Biogeochemical impacts of glacial meltwaters across a High Arctic watershed (Lake Hazen, Nunavut, Canada). University of Alberta. https://doi.org/https://doi.org/10.7939/R3XG9FS81

Stephens, G.L., Vane, D.G., Tanelli, S., Im, E., Durden, S., Rokey, M., Reinke, D., Partain, P., Mace, G.G., Austin, R., 2008. CloudSat mission: Performance and early science after the first year of operation. J. Geophys. Res. Atmos. 113.

Stout, J.E., 2001. Dust and environment in the southern high plains of North America. J. Arid Environ. 47, 425–441.

Tang, M., Cziczo, D.J., Grassian, V.H., 2016. Interactions of water with mineral dust aerosol: water adsorption, hygroscopicity, cloud condensation, and ice nucleation. Chem. Rev. 116, 4205–4259.

Vincent, R.F., 2018. The effect of Arctic dust on the retrieval of satellite derived sea and ice surface temperatures. Sci. Rep. 8, 1–10.

Wang, Z., Vane, D., Stephens, G., Reinke, D., 2012. Level 2 combined radar and lidar cloud scenario classification product process description and interface control document. JPL Rep 22.

Washington, R., Todd, M.C., 2005. Atmospheric controls on mineral dust emission from the Bodélé Depression, Chad: The role of the low level jet. Geophys. Res. Lett. 32.

Weinzierl, B., Petzold, A., Esselborn, M., Wirth, M., Rasp, K., Kandler, K., Schuetz, L., Koepke, P., Fiebig, M., 2009. Airborne measurements of dust layer properties, particle size distribution and mixing state of Saharan dust during SAMUM 2006. Tellus B Chem. Phys. Meteorol. 61, 96–117.

Whicker, J.J., Breshears, D.D., Wasiolek, P.T., Kirchner, T.B., Tavani, R.A., Schoep, D.A., Rodgers, J.C., 2002. Temporal and spatial variation of episodic wind erosion in unburned and burned semiarid shrubland. J. Environ. Qual. 31, 599–612.

Winker, D.M., Vaughan, M.A., Omar, A., Hu, Y., Powell, K.A., Liu, Z., Hunt, W.H., Young, S.A., 2009. Overview of the CALIPSO mission and CALIOP data processing algorithms. J. Atmos. Ocean. Technol. 26, 2310–2323.

Woo, M.K., Edlund, S.A., Young, K.L., 1991. Occurrence of early snow-free zones on Fosheim Peninsula, Ellesmere Island, Northwest Territories. Curr. Res. Part B, Geol. Surv. Canada Pap. 91, 9–14.

Xie, Y., Zhang, W., Qu, J.J., 2017. Detection of asian dust storm using MODIS measurements. Remote Sens. 9, 869.

Zwaaftink, C.D.G., Grythe, H., Skov, H., Stohl, A., 2016. Substantial contribution of northern high-latitude sources to mineral dust in the Arctic. J. Geophys. Res. Atmos. 121, 13–678.

4. Conclusions

Paper 1 was an original and, we believe, an innovative article published in Atmospheric Environment. It deals with an extreme smoke event observed over Eureka in August of 2017. First and foremost this paper was original in terms of the event it reported (the largest optical depth ever recorded over Eureka) and in terms of the instrumental infrastructure and expertise that we developed over many years at Eureka. The paper was also original in terms of the production of a 10-year τ_f (fine mode optical depth) smoke climatology (based on AEROCAN / AERONET data collected at our two sites in Eureka) that had to be pre-filtered to exclude events such as the 2008 and 2009 Kasatochi and Sarychev stratospheric intrusion of fine mode sulphates. An additional and original constraint on the labelling of τ_f events as smoke events was the correlation between τ_f and CO abundance measured using a FTIR[13] (CO being a classical smoke product): the level of correlation observable in Figure 5 of that paper is to our knowledge unprecedented and, in the presence of severe variations of cloud optical depth, speaks to the reliability of the retrieval method (the SDA retrieval of AERONET). To demonstrate the extreme nature of the event we employed a "peak over threshold" (POT) analysis of individual τ_f peaks during our 10-year sampling period. This process involved a careful analysis of all significant smoke events during that period and the conversion of that manual analysis into an automatic routine for extraction of all smoke events above a certain τ_f threshold. This generated a distribution of extreme smoke events from which the statistical inference of a significant extreme could be drawn. Conversely, the August 2017 event was not found to be an extreme event in terms of a simple monthly average approach: this observation is consistent with the notion that extreme event statistics were needed to demonstrate the uniqueness of the event.

Paper 2 was arguably the most significant and original contribution. It involved the successful application of remote sensing techniques to detect a low-altitude dust plume over Lake Hazen in the high-Arctic[14] using a diverse array of passive and active, satellite-based remote sensing techniques. We are not aware of any published remote sensing investigations of local Arctic dust: remote sensing measuring conditions over a complex surface of snow, ice and dust are marginal at best. We exploited MISR multi-angle imaging capabilities and multi-spectral (visible to thermal

[13] Fourier Transform Infrared Radiometer

[14] Located on Ellesmere Island, NV, about 300 km northeast of our PEARL observatory at Eureka.

infra-red) imaging capabilities (MODIS) as well as the particle size dependant profiling capabilities of active sensors (the CALIOP lidar and the CloudSat radar) to identify, localize and characterize the key physical and optical properties of the dust plume. This process was accomplished in spite of the fact that the remote sensing products of all these sensors were not adapted to Arctic conditions (none of those products indicated the dust nature, let alone the aerosol nature of the plume). In the end, we succeeded in characterizing the upper plume thickness (the region of highest signal to noise) in terms of 532 nm optical depth (~ 0.7) and the effective radius of the plume particles (between 18 and 25 μm in radius; what the dust community characterize as "giant" dust particles). Such local dust events, viewed as an ensemble of regular late spring, early fall phenomena over the Arctic, have been recognized in recent years as important contributors to Arctic-wide aerosol dynamics and associated radiative forcing effects. In the latter case, we produced MODIS-derived imagery over Lake Hazen and Ellesmere Island that demonstrated the browning (albedo reducing) effects that were likely due to drainage-flow dust events; the impact of absorbing dust on snow and ice melt at high-latitudes has been recognized as a potentially important positive feedback effect (as noted by Bullard et al. 2016, a key citation of Paper 2).

5. Future work

We seek to publish another article in order to report on how the difference between the τ_c (coarse mode optical depth) retrievals of the PEARL and OPAL AERONET instruments (one at seal-level and the other at 610 meters ASL) was well correlated with ground-based, volumetric (volume sampling) coarse-mode PSD measurements of local dust acquired by an APS (Aerodynamic Particle Sizer). This result, aside from generating another important example of local Arctic dust, is unique in demonstrating that τ_c differences (differences well below the nominal optical depth error of the two instruments employed) still showed significant correlation with independent surface measurements.

We hope to publish another article on the correlation between volumetric, fine mode PSD measurements acquired with an SMPS (Scanning Mobility Particle Sizer), OPAL τ_f retrievals and CRL lidar profiles at Eureka. This analysis showed different instances of moderate to strong correlations that were however dispersed in position on a general scattergram of τ_f vs SMPS fine mode volume. The CRL profiles allowed us to characterize the different linear tendencies in terms

of different aerosol profiles (from high-altitude smoke plumes which produced a linear tendency with very large slope due to weak SMPS smoke signal at the SMPS elevation) to boundary layer, Arctic haze aerosols which produced much more moderate slopes resulting form much stronger SMPS signals).

Other events that we have been actively investigating include smoke and volcanic sulphate intrusions into the Arctic that occurred during the extreme stratospheric loading of the summer of 2019 and, inspired by modelled (GEOS-Chem) sea-salt AOD simulations of an ubiquitous yearly climate event (the wind inducing winter low in the north Atlantic) sea-salt events in the neighbourhood of Ny Alesund. We also compared and analyzed the combination of ground-based data at other sites: notably at Barrow, Alaska where we investigated the profiles of Asian dust aerosols (using the University of Wisconsin's high spectral resolution lidar) as well as the positive correlation between course mode AODs from the AERONET site at Barrow and wind speed (the latter parameter acting as a proxy for sea-salt aerosols). In all these investigations we made, at every opportunity, generous use of satellite derived profiles and AODs from the CALIOP lidar on the A-train constellation as well as other remote sensing data such as MODIS and MISR imagery. These specific investigations are indicators of where our research efforts are at present and where our future research into natural aerosols over the Arctic is going.

6. References

The references below were cited in the Introduction and Conclusions sections

AboEl-Fetouh, Y., O'Neill, N. T., Ranjbar, K., Hesaraki, S., Abboud, I., Sobolewski, P.S. (2020). Climatological-scale analysis of intensive and semi-intensive aerosol parameters derived from AERONET retrievals over the Arctic. *Journal of Geophysical Research: Atmospheres,*

Breider, T. J., L. J. Mickley, D. J. Jacob, Q. Wang, J. A. Fisher, R. Y. W. Chang & B. Alexander (2014). Annual distributions and sources of Arctic aerosol components, aerosol optical depth, and aerosol absorption. *Journal of Geophysical Research: Atmospheres,* 119**,** 4107-4124.

Bullard, J. E., Baddock, M., Bradwell, T., Crusius, J., Darlington, E., Gaiero, D., … McCulloch, R. (2016). High-latitude dust in the Earth system. *Reviews of Geophysics*, *54*(2), 447–485.

Deirmendjian, D. (1969). *Electromagnetic scattering on spherical polydispersions*. Rand Corp Santa Monica CA.

Di Pierro, M., Jaeglé, L., Eloranta, E. W., & Sharma, S. (2013). Spatial and seasonal distribution of Arctic aerosols observed by CALIOP (2006-2012). *Atmospheric Chemistry & Physics Discussions*, *13*(2).

Fromm M, Lindsey DT, Servranckx R, Yue G, Trickl T, Sica R, Doucet P, Godin-Beekmann S. (2010). The untold story of pyrocumulonimbus. Bulletin of the American Meteorological Society. 91(9):1193-210.

Jaeglé, L., Quinn, P. K., Bates, T. S., Alexander, B., and Lin, J.-T. (2011). Global distribution of sea salt aerosols: new constraints from in situ and remote sensing observations, *Atmospheric Chemistry and Physics*, 11, 3137–3157, doi:10.5194/acp-11-3137-2011.

Hansen, J. E. & L. D. Travis (1974). Light scattering in planetary atmospheres. *Space Science Reviews,* 16**,** 527-610.

Hesaraki, S., Neill, N. T. O., Lesins, G., Saha, A., Randall, V., Fioletov, V. E., … Abboud, I. (2017). Comparisons of a Chemical Transport Model with a Four-Year (April to September) Analysis of Fine- and Coarse-Mode Aerosol Optical Depth Retrievals Over the Canadian Arctic. *Atmosphere-Ocean*, 55(4–5), 213–229. https://doi.org/10.1080/07055900.2017.1356263

Hinds, W. C. (1999). Aerosol Technology: Properties, Behavior, and Measurement of Airborne Particles (Second Edi.). John Wiley & Sons, Inc.

Hoffmann, A., C. Ritter, M. Stock, M. Maturilli, S. Eckhardt, A. Herber, and R. Neuber (2010), Lidar measurements of the Kasatochi aerosol plume in August and September 2008 in Ny-Ålesund, Spitsbergen, J. Geophys. Res., 115, D00L12, doi:10.1029/2009JD013039.

IPCC (2013). Climate Change 2013: The Physical Science Basis. Contribution of Working Group I to the Fifth Assessment Report of the Intergovernmental Panel on Climate Change. Intergovernmental Panel on Climate Change, Working Group I Contribution to the IPCC Fifth Assessment Report (AR5)(Cambridge Univ Press, New York), p. 1535.

Law, K. S. et Stohl, A. (2007). Arctic air pollution: *Origins and impacts. science*, vol. 315, n°5818, p. 1537‑1540.

Myhre, C.L., Toledano, C., Myhre, G., Stebel, K., Yttri, K.E., Aaltonen, V., Johnsrud, M., Frioud, M., Cachorro, V., Frutos, A. de (2007). Regional aerosol optical properties and radiative impact of the extreme smoke event in the European Arctic in spring 2006. *Atmospheric Chemistry and Physics*. 7, 5899–5915.

O'Neill, N. T., Eck, T. F., Holben, B. N., Smirnov, A., Dubovik, O. et Royer, A. (2001). Bimodal size distribution influences on the variation of Angstrom derivatives in spectral and optical depth space. *Journal of Geophysical Research: Atmospheres*, vol. 106, n°D9, p. 9787‑9806.

O'Neill, N. T., T. Eck, A. Smirnov, B. Holben & S. Thulasiraman (2003). Spectral discrimination of coarse and fine mode optical depth. *Journal of Geophysical Research: Atmospheres,* 108.

O'Neill, N. T., Perro, C., Saha, A., Lesins, G., Duck, T. J., Eloranta, E. W., Nott, G. J., et al. (2012). Properties of Sarychev sulphate aerosols over the Arctic. *Journal of Geophysical Research: Atmospheres*, vol. 117, n°D4.

Pitts, M. C., L. R. Poole, A. Dörnbrack, L. W. Thomason (2011). The 2009–2010 Arctic polar stratospheric cloud season: a CALIPSO perspective, *Atmospheric Chemistry and Physics*, 11, 2161-2177.

Quinn, P. K., Bates, T. S., Baum, E., Doubleday, N., Fiore, A. M., Flanner, M., Fridlind, A., et al. (2008). Short-lived pollutants in the Arctic: their climate impact and possible mitigation strategies. *Atmospheric Chemistry and Physics,* vol. 8, n°6, p. 1723‑1735.

Rose, W., Y. Gu, I. Watson, T. Yu, G. Blut, A. Prata, A. Krueger, N. Krotkov, S. Carn & M. Fromm (2003) The February–March 2000 eruption of Hekla, Iceland from a satellite perspective. *Volcanism and the Earth's Atmosphere***,** 107-132.

Serreze, M. C., Holland, M. M. et Stroeve, J. (2007). Perspectives on the Arctic's shrinking sea-ice cover. *science*, vol. 315, n°5818, p. 1533‑1536.

Shaw, G. E. (1995). The Arctic haze phenomenon. *Bulletin of the American Meteorological Society*, vol. 76, n°12, p. 2403‑2414.

Shindell, D. et Faluvegi, G. (2009). Climate response to regional radiative forcing during the twentieth century. *Nature Geoscience*, vol. 2, n°4, p. 294.

Stohl, A. (2006). Characteristics of atmospheric transport into the Arctic troposphere. *Journal of Geophysical Research: Atmospheres*, *111*(D11).

Stone, R. S., Sharma, S., Herber, A., Eleftheriadis, K., & Nelson, D. W. (2014). A characterization of Arctic aerosols on the basis of aerosol optical depth and black carbon measurements. Elementa: *Science of the Anthropocene*, 2, 1–22. https://doi.org/10.12952/journal.elementa.000027

Tomasi C, Vitale V, Lupi A, Di Carmine C, Campanelli M, Herber A, Treffeisen R, Stone RS, Andrews E, Sharma S, Radionov V. (2007). Aerosols in polar regions: A historical overview

based on optical depth and in situ observations. *Journal of Geophysical Research: Atmospheres*. 112(D16).

Tomasi, C., Kokhanovsky, A. A., Lupi, A., Ritter, C., Smirnov, A., O'Neill, N. T., Stone, R. S., et al. (2015). Aerosol remote sensing in polar regions. *Earth-Science Reviews*, vol. 140, p. 108 ‑157.

von Hardenberg, J. V, Vozella, L., Tomasi, C., Vitale, V., Lupi, A., Mazzola, M., Van Noije, T.P.C., Strunk, A., Provenzale, A. (2012). Aerosol optical depth over the Arctic: a comparison of ECHAM-HAM and TM5 with ground-based, satellite and reanalysis data. *Atmospheric Chemistry and Physics.* 12.

Warneke, C., Froyd, K. D., Brioude, J., Bahreini, R., Brock, C. A., Cozic, J., De Gouw, J. A., et al. (2010). An important contribution to springtime Arctic aerosol from biomass burning in Russia. *Geophysical Research Letters*, vol. 37, n°1.

Xie, Y., Li, Z., Li, L., Wagener, R., Abboud, I., Li, K., … Xu, H. (2018). Aerosol optical, microphysical, chemical and radiative properties of high aerosol load cases over the Arctic based on AERONET measurements. *Scientific Reports*, 8(1), 1–9. https://doi.org/10.1038/s41598-018-27744-z

Zwaaftink, C. D. G., Grythe, H., Skov, H., & Stohl, A. (2016). Substantial contribution of northern high-latitude sources to mineral dust in the Arctic. *Journal of Geophysical Research: Atmospheres*, *121*(22), 13–678.